

1 We are grateful to the two reviewers for their comments and have made all suggested
2 revisions accordingly. We also addressed the comment of Dr. Fyke and corrected our
3 reference mistake. Below please find responses to all reviewer's comments. Our responses
4 are highlighted in yellow. The tracked changes version of the paper follow,
5

Interactive comment on “Investigating the Local Scale Influence of Sea Ice on Greenland Surface Melt” by Julienne C. Stroeve et al.

Anonymous Referee #1

Received and published: 5 June 2017
June 5, 2017

I have read the manuscript “Investigating the local influence of sea ice on Greenland surface melt” by J.C. Stroeve et al. This work evaluates statistical and physical links between Arctic sea ice conditions and subsequent melt events observed over the Greenland Ice Sheet.

Through a statistical framework, the authors find strong covariability between Baffin Bay and Davis Strait melt and freeze onset and ice sheet melt occurrence within close spatial proximity to the aforementioned oceanic regions. The physical associations presented between local sea ice cover and the ice sheet appear to substantiate the author’s statistical findings. In particular, composite turbulent flux and wind field analyses show transport of warm, moist air from the ocean (evident in early melt years) onto the ice sheet that subsequently enhance glacial melt, especially at lower elevations around the western and southern margins.

Overall, this manuscript is well-written and concise and I believe the quality of analyses presented are consistent with manuscripts published in *The Cryosphere*. This paper would make a contribution to the growing body of local/regional sea ice-ice sheet inter- actions within a rapidly changing North Atlantic Arctic environment. I would recommend acceptance pending the completion of a relatively small number of revisions, which I have detailed below by line numbers in the submitted manuscript.

Minor Comments:

6 Line 56: Add “...and mid-tropospheric height” after SLP to reflect coincident mid-level
7 circulation changes in the Arctic. Papers such as Bezeau et al (2015) *Int J Clim*
8 (doi:10.1002/joc.4000) could also be cited here.

9 Thank you for bringing this new reference to our attention. We have made the suggested
10 additions.

11 Line 60: Relevant recent work by Ballinger et al. (2017) *Clim Dyn* (doi:10.1007/s00382-
12 017-3583-3) similarly notes poleward advection of warm air masses delays autumn freeze
13 onset in Baffin Bay, and impacts Greenland coastal temperature signals, and would
14 appropriately fit here.

15 Thank you for bringing this new reference to our attention. We have added the citation.

16

Line 129: Do MAR 850 hPa winds, which use ERA products, compare more favorably
relative to observations than MERRA low-level winds? As 500 hPa geopotential height
and 10m winds are obtained from MERRA it would seem appropriate to use a similar
product for 850 hPa winds.

17 We had at one point used 10 m and 850 hPa winds in Fig. 11 but did not keep them in the

end. It looks like we forgot to remove that from the data section so this becomes a non-issue. However, we used 10 m wind in Fig. 12 from MERRA-2.

Lines 132-133: Clarify whether MAR output for 2002 is forced by ERA-40 and ERA-I or just one of these datasets.

It is forced by ERA-40 from 1979-2002 and by ERA-I from 2002 to 2015.

Line 158: List the threshold of statistical significance used throughout the paper.

Done

Line 193: Change “didn’t” to “did not”

Done

18 Lines 195-198: The authors should explicitly state what advantages SVD offers beyond
more traditional bivariate correlation between two data fields? Such justification would
be helpful given that simple and partial correlation techniques are also utilized in the paper.

19 The advantage of singular value decomposition is that it is able to maximum the
20 covariance between the two fields to explicitly show the structure of the covariability,
21 and also provides subsequent orthogonal modes of covariability (not as relevant for
22 this paper since we only show the leading mode) that are by definition unrelated to
23 the leading mode.

24
25 Line 239: Should this be Eq. 1? I do not see a second equation listed in the manuscript.
26 Thank you, this was a typo now corrected.

27
28 Line 241-242: When compositing by anomalous melt and freeze years using a +/-1
29 sigma threshold, it appears that only 3 early melt and 4 late melt onset are considered
30 (as mentioned in Fig 12). If the sigma threshold is relaxed to increase sample size
31 (perhaps to +/-0.75 sigma) does this substantially alter lower tropospheric wind
32 patterns?

33 The 1σ threshold gives a different number of years for each region. In Figure 12 we
34 just show the Baffin Bay region which does have only a few years with 1s differences
35 in MO. If we relax to 0.75σ , the number of years anomalous in the AIRS time-period
36 did not change. Ideally, we need a longer time-series of data from AIRS to look at
37 including even more anomalous years in the composite.

38
39 Line 280: Change “hPA” to “hPa.”

40 Done

41
42 Table 3: Does simple correlation reference a specific technique (i.e. Pearson’s or
43 Spearman’s)? Clarify this in the caption and table.

44 This was a Pearson’s correlation, this has now been added to the table caption.

45
46 Figures 9a/b: Graphic is somewhat confusing with time series plots stacked directly
47 on top of each other. I would suggest that panels be clearly separated into a two-panel
48 plot (labeled as a-d for instance) with y axis labeled accordingly on the correlation
49 time series.

50 We have changed the figures accordingly to make them Figures A-D. Here are the
51 captions for each:
52 Figure 9.
53 a) Baffin Bay SIC region latent heat flux (W/m²) from early minus late MO years
54 (black line) and Baffin Bay GrIS region specific humidity (g/kg) from early minus late
55 MO years (red line).
56 b) Week Lag-1 week lagged running correlations (between 0.5 and 1.0) for early MO
57 years latent heat flux from Baffin Bay and specific humidity from GrIS (blue line) and
58 late MO latent heat flux from Baffin Bay and specific humidity GrIS years (green line).
59 c) Baffin Bay SIC region sensible heat flux (W/m²) from early minus late MO years
60 (black line) and Baffin Bay GrIS region air temperature (K) from early minus late MO
61 years (red line).
62 d) Week Lag-1 week lagged running correlations (between 0.5 and 1.0) for early MO
63 years sensible heat flux from Baffin Bay and air temperature from GrIS (blue line) and
64 late MO sensible heat flux from Baffin Bay and air temperature GrIS years (green line).
65 In a-d) Dotted vertical lines represent the aver early MO date for Baffin Bay (dotted
66 blue), and average late MO date for Baffin Bay (dotted blue, red highlight), average
67 early MO date from GrIS (dotted green), and average late MO date form GrIS (dotted
68 green, orange highlight).
69
70 Figure 12: Are these winds from AIRS or MERRA? The manuscript explicitly mentions
71 use of MERRA 10m winds (line 160), but not from AIRS.
72 Correct, these winds are from MERRA2 in Figure 12. The reason why we do not use
73 AIRS in this figure is because AIRS does not produce a wind product and there are no
74 other satellite based wind products in the Arctic to our knowledge.
75 New Caption: Figure 12. Wind vectors and speeds at 10 meters from MERRA2 during
76 4 early melt years over Baffin Bay (top panel) and 3 late sea ice melt years (bottom
77 panel). Smaller figures superimposed on the wind maps show the sea ice
78 concentration (%) for that day.
79

80
81 ***Interactive comment on “Investigating the Local Scale Influence of Sea Ice on***
82 ***Greenland Surface Melt” by Julienne C. Stroeve et al. Anonymous Referee #2***
83

84 Received and published: 4 July 2017

85 **General comments**

86 The study documents a statistical investigation and possible dynamical explanations of the
87 covariance between sea ice concentration and the surface melt of Greenland Ice Sheet. The
88 purpose is to demonstrate the impact of local changes of sea ice around Greenland on the
89 ice sheet surface mass balance. The manuscript is well structured and the conclusions are
90 clear based on the results of the analyses. The topic is interesting and relevant within the
91 scope of The Cryosphere, and thus, with the changes suggested below, it should be
92 acceptable for publication.

93

94 **Specific comments**

95 L254: you stated that the leading SVD mode explains 62% covariance between SIC C1
96 TCD and GrIS melt water production in June. This number might be misleading if
97 there is only a very small amount of covariance between these two fields. In this case,
98 the ‘normalized squared covariance’ (NSC) should be included as well (see details in
99 Wallace et al., 1993 Journal of Climate).

100 The SVD was the first step for that particular analysis because it showed us the actual
101 regions where we could be seeing a causal relationship based the locations of (maybe
102 somewhat confusingly) significant correlations in the heterogeneous correlation
103 maps. From there, we isolated two regions, Baffin Bay and Beaufort Sea, and did a
104 similar analysis using partial correlation. Correlation is limited because you can't have
105 two fields, so I took the spatial average of Baffin and Beaufort and correlated (and
106 partial-correlated) that time series with the time series of melt at each grid point in
107 Greenland.

108

109 Thank you for pointing out these references to the NSC. We added reference in the
110 methods to the NSC: The normalized squared covariance (NSC) associated with each
111 pair of spatial patterns indicates the total strength of this relationship [Wallace et al.
112 1993], with values greater than approximately 0.10 considered to indicate a
113 significant relationship [Riaz et al. 2017].

114

115 We further calculated this normalized squared covariance as suggested. The NSC
116 between 500 hPa heights and melt is:

117 June: 0.191

118 July: 0.111

119 August: 0.093

120

121 For sea ice and melt, NSC is:

122 June: 0.099

123 July: 0.081

124 August: 0.066

125

126 So there generally is a significant coupling between the ice sheet melt and height

127 fields as we expect, but it is less significant between ice sheet melt and sea ice, which
128 is more important. We were already thinking that this relationship is rather tenuous,
129 and this is just further support for that idea. We additionally added the NSC values to
130 Figure 3.

131
132 There is very little information employing NSC, and how hard a threshold of 0.10 is,
133 but we do believe that the reviewer's comment on 482-492 is justified then and the
134 fact that we lose much of the correlation between sea ice/ice melt after removing the
135 GBI warrants mention of this 0.099 value to say that the coupling between these two
136 fields is relatively weak. We added a statement in the Discussion to highlight this
137 result:

138 *This explanation is supported by the relatively weak value of NSC for June GrIS melt and*
139 *SIC, which nearly doubles to 0.191 in the SVD analysis of 500 hPa geopotential heights*
140 *instead of SIC.*

141 L262: Figure 3(i) does not show any significant HC values, so it should not be included in
142 this sentence.

143 That is correct and it is a relic of the old figures, so we removed reference to Fig. 3i.

144 L482-492: after you remove the impact of Greenland Blocking, the Baffin Bay SIC
145 influence becomes much smaller. This may be because the overall coupling between the
146 SIC and GrIS surface melt is not significant. Thus, the additional calculation of NSC
147 mentioned above will probably help you to interpret the results.

148 See our response to previous comment.

149
150 L543-552: you wanted to show that during the early MO years over the sic ice, the wind is
151 blowing from the open water areas onto the GrIS, but the plots in Figure 12 are exactly the
152 opposite. For example, the figures in upper panel, the winds are offshore along the west
153 coast of Greenland in all three cases.

154 That was a typo on our part, this has now been corrected. The winds do indeed show
155 onshore flow along the west coast of Greenland during early MO years. The figures have
156 been made larger so that this is seen easier.

157
158 L60: can you please tell more details of how you calculated the linear trends? Which
159 method you used to do the significant test? In the legend, you should also specify which
160 confidence level you used.

161 Done, linear trends were computed using least square regression and evaluated using a
162 student T-test at 95% confidence.

163
164 L66: maybe you can indicate the weeks with significant trends on different lines?
165 We feel this will make the figure too cluttered as it is a busy figure already. The figure is
166 more for illustration, showing how trends vary as a function of time of year for the
167 different sectors around Greenland.

168
169 L71: please specify the confidence level you used. Maybe use 'a, b and c' to mark the
170 figures in order to be consistent with other figures? Or, it should be 'left, middle and right',
171 but not 'top, middle and bottom'.
172 Yes thank you, this has been corrected.

175
176 Figure 12: please specify what is the parameter shown with blue and red colors. I guess it's
177 SIC, and if so, you should give a separated color bar as well. Please make the color bars
178 and the wind vectors bigger and clearer. The readers can hardly see them.
179 We made the figures larger and added the SIC color bar.

180 **Investigating the Local Scale Influence of Sea Ice on**
181 **Greenland Surface Melt**

182
183 Julianne C. Stroeve^{1,2}, John R. Mioduszewski³, Asa Rennermalm⁴, Linette N. Boisvert⁵,
184 Marco Tedesco⁶, and David Robinson⁴

185 ¹National Snow and Ice Data Center, Cooperative Institute for Research in Environmental
186 Sciences, University of Colorado, 449 UCB, Boulder, CO 80309, USA.

187 ²Centre for Polar Observation and Modelling, University College London, Department of
188 Earth Sciences, Gower Street, London, WC1E6BT, UK.

189 ³Center for Climatic Research, University of Wisconsin – Madison, 1225 W. Dayton St.,
190 Madison, WI 53706, USA.

191 ⁴Department of Geography, Rutgers, The State University of New Jersey, 54 Joyce Kilmer
192 Avenue, Piscataway NJ 08854-8045, USA.

193 ⁵NASA Goddard Space Flight Center, Greenbelt, MD, 20771, USA.

194 ⁶Lamont, Columbia University

195

196 **Abstract**

197 Rapid decline in Arctic sea ice cover in the 21st century may have wide-reaching effects on
198 the Arctic climate system, including the Greenland ice sheet mass balance. Here, we
199 investigate whether local changes in sea ice around the Greenland ice sheet have had an
200 impact on Greenland surface melt. Specifically, we investigate the relationship between sea
201 ice concentration, the timing of melt onset and open water fraction surrounding Greenland
202 with ice sheet surface melt using a combination of remote sensing observations, and
203 outputs from a reanalysis model and a regional climate model for the period 1979 - 2015.
204 Statistical analysis points to covariability between Greenland ice sheet surface melt and sea
205 ice within Baffin Bay and Davis Strait. While some of this covariance can be explained by
206 simultaneous influence of atmospheric circulation anomalies on both the sea ice cover and
207 Greenland melt, within Baffin Bay we find a modest correlation between detrended melt
208 onset over sea ice and the adjacent ice sheet melt onset. This correlation appears to be
209 related to increased transfer of sensible and latent heat fluxes from the ocean to the
210 atmosphere in early sea ice melt years, increasing temperatures and humidity over the ice
211 sheet that in turn initiate ice sheet melt.

212

Deleted: a
Deleted: nd

215 1. Introduction

216 The shrinking sea ice cover is one of the most striking features of Arctic climate change
217 [e.g. Stroeve *et al.*, 2012; Serreze *et al.*, 2007]. Since the late 1970s, the sea ice extent (SIE)
218 has declined by more than 40% in September, with smaller, yet statistically significant
219 negative trends in other months. These negative trends have been linked to the observed
220 increases in atmospheric CO₂, with the prospect of the Arctic Ocean becoming seasonally
221 ice free before the middle of this century if current emission rates continue [Notz and
222 Stroeve, 2016]. At the same time, the Greenland ice sheet (GrIS) has experienced increased
223 summer melt [e.g. Tedesco *et al.*, 2011; Fettweis *et al.*, 2011] and an increasingly negative
224 mass balance [Khan *et al.*, 2015]. While earlier studies found GrIS mass loss to be
225 balanced by ice discharge and ice melt [van den Broeke *et al.*, 2009], newer evidence
226 shows surface melting is now contributing 84% to the mass loss since 2009 [Enderlin *et*
227 *al.*, 2014]. It has further been suggested that surface melting will dominate Greenland's
228 contribution to sea level rise throughout the rest of this century [Enderlin *et al.*, 2014; Fyke
229 *et al.*, 2014a]. Similar to the sea ice environment, an anthropogenic signal has been
230 identified in the observed changes of GrIS surface mass balance (SMB) [Fyke *et al.*,
231 2014b].

232 While both the GrIS and sea ice environments are responding to anthropogenic
233 warming [Hanna *et al.*, 2008], changes in atmospheric circulation patterns that favor
234 increased sea ice loss and GrIS melt have also played a role. Analysis of summer (JJA) sea
235 level pressure (SLP) mid-tropospheric reveal statistically significant increases over
236 Greenland and north of the Canadian Arctic Archipelago coupled with significant negative
237 trends over northern Eurasia and Canada from 1979 to 2014 [Serreze *et al.*, 2016; Bezeau
238 *et al.*, 2014], dominated by a clear shift in the last decade (2005 to 2014) towards large
239 positive SLP anomalies over the central Arctic Ocean and Greenland. This pattern favors
240 both summer sea ice loss [e.g. Wang *et al.*, 2009; Ogi and Wallace, 2007] as well as
241 Greenland surface melt [Hanna *et al.* 2013; Mioduszewski *et al.*, 2016; Ballinger *et al.*,
242 2017]. Additionally, advection of warm and humid air masses appears to be the primary
243 factor initiating sea ice melt onset [Boisvert and Stroeve, 2015; Mortin *et al.*, 2016].
244 Anomalous GrIS melting also appears to coincide with increasing water vapor transport to
245 the ice sheet [Mattingly *et al.*, 2016]. Thus, it is not surprising that there is a strong inverse
246 correlation between GrIS melt intensity (defined by Tedesco *et al.*, 2007) and the pan-
247 Arctic September SIE ($r = -0.83$ from 1979 to 2015) [Figure 1]. Detrended data reveal a
248 substantially weaker inverse relationship ($r = -0.27$), yet the year-to-year variability
249 between September SIE and GrIS melt remains highly correlated ($r = -0.69$). This would
250 suggest that atmospheric processes fostering a high melt year also tend to foster more
251 summer sea ice loss and vice versa.

252 What about local-scale feedbacks? Changes in sea ice have strong local-scale
253 influences on the Arctic climate through enhanced transfer of heat and moisture between
254 the ocean and atmosphere, resulting in amplified Arctic warming [e.g. Serreze *et al.*, 2009;
255 Screen and Simmonds, 2010]. This is mostly manifested during the cold season, as
256 warming of the ocean mixed layer during summer results in increased sensible and latent
257 heat transfer from the ocean to the atmosphere [Boisvert *et al.*, 2015]. Other studies have
258 linked sea ice loss to atmospheric warming in surrounding areas during other times of the
259 year as well [Comiso *et al.*, 2002; Hanna *et al.*, 2004; Bhatt *et al.*, 2010, Serreze *et al.*,
260 2011]. Sea ice loss is additionally tied to increased tropospheric moisture, precipitation,
261 cloud cover, surface temperature, and decreased static stability [Deser *et al.*, 2000; Rinke et

Formatted: Font:Italic

Formatted: Font:Italic

262 *al.*, 2006; *Francis et al.*, 2009; *Serreze et al.*, 2009; *Kay et al.*, 2011; *Screen and*
263 *Simmonds*, 2010; *Stroeve et al.*, 2011; *Overland and Wang*, 2010; *Cassano et al.*, 2014].
264 Water vapor or moisture increases surface melting through its role in cloud formation and
265 as a greenhouse gas, results in increased downward longwave radiation and precipitation
266 [Bennartz *et al.*, 2013, *Doyle et al.*, 2015, *van Tricht et al.*, 2016].

267 This study examines whether or not local changes in the sea ice environment around
268 Greenland are already impacting GrIS meltwater production and therefore SMB variations.
269 First, we identify regions of SIC and GrIS melt covariability by applying the singular value
270 decomposition method. We hypothesize that regions of covariability will have consistent
271 trends in sea ice cover and melt production, as well as consistent trends in spring melt onset
272 and fall freeze up. As a second step, this hypothesis is examined with a spatial analysis of
273 trends for the entire study domain. Third, we investigate if a plausible mechanism for local
274 scale influence between SIC and GrIS is present. Specifically, we hypothesize that the
275 mechanism for the local scale influence is controlled by positive turbulent fluxes from the
276 SIC regions. Therefore, anomalous turbulent fluxes should be larger in years with early sea
277 ice melt onset than in later years in regions of covariability. In turn, these turbulent heat
278 fluxes should result in increased specific humidity and near surface temperature over the
279 GrIS, which should be reflected in positive net longwave radiation anomalies. Finally, a
280 detailed analysis, restricted to the region with evidence of local scale influence, is
281 performed. In this analysis, we examine the hypotheses that the timing of turbulent heat
282 flux anomaly perturbations over reduced sea ice areas proceeds changes in GrIS humidity
283 and temperature, and that wind patterns in early melt onset years are favorable for turbulent
284 heat flux transport from the ocean to the ice sheet. Finally, correlation and partial
285 correlation analysis is used to examine the influence of large scale atmospheric circulation
286 (here represented by the Greenland Blocking Index).

287 **2. Data**

288 **2.1 Sea Ice and Ice Sheet Data**

289 Sea ice and Greenland melt extent/area calculations rely on algorithms applied to
290 satellite passive microwave data from the Nimbus-7 Scanning Multichannel Microwave
291 Radiometer (SMMR: 1978-1987) and the DMSP Special Sensor Microwave/Imagers
292 (SSM/I and SSMIS: 1987-present). Specifically, we use several sea ice metrics derived
293 from the NASA Team SIC algorithm [*Cavalieri et al.*, 1996, updated 2008] and distributed
294 by the National Snow and Ice Data Center (NSIDC). The data set spans October 1978 to
295 present, providing daily (or every other day during the SMMR era) SIC estimates. Using
296 the SIC, we additionally calculate the open water fraction (OWF) as well as the length of
297 the ice-free season, defined as the number of days each year with ice concentration less
298 than 15% [see *Parkinson*, 2014].

299 Changes in the timing of melt onset (MO) and freeze-up (FO), in addition to total melt
300 season length over sea ice, are computed following *Markus et al.* [2009]. This study uses
301 an updated version of the algorithm that bias corrects for intersensor calibration issues
302 found between the F17 and F13 sensor and evaluates early melt onset (EMO),
303 corresponding to the first day of MO, the continuous MO and the continuous FO.

304 GrIS melt extent is an estimate of the daily spatial extent of wet snow using the *Mote et*
305 *al.* [2014] algorithm and distributed by NSIDC. From the binary melt/no melt
306 classification, GrIS MO and FO dates were calculated for each pixel and each year from

307 1979 to 2015. We defined the start of the MO and FO as the first occurrence of a 5-day
308 continuous melt or freeze-up period. Melt duration was calculated as the number of days
309 between MO and FO. EMO was also determined and defined as the first time a spurious
310 melt event lasting at least one day was recorded.

311 Besides mapping the GrIS melt extent and timing of MO and FO, we use meltwater
312 production and 850 hPa wind as simulated by Modèle Atmosphérique Régional (MAR)
313 v3.2 regional climate model [Tedesco *et al.*, 2013]. MAR is a three-dimensional coupled
314 atmosphere-land surface model that uses reanalysis data at its lateral boundaries. In this
315 study, MAR is forced with data from ERA-40 for the period 1979–2002 and ERA-Interim
316 for the period 2002–2015 and outputs are produced on a polar stereographic projection
317 with an approximate grid cell size of 25 x 25 km to match the passive microwave-derived
318 fields. MAR’s atmospheric model is coupled to the 1-D Surface Vegetation Atmosphere
319 Transfer scheme, SISVAT [Gallée and Schayes, 1994; De Ridder and Gallée, 1998], which
320 simulates surface properties and the exchange of mass and energy. SISVAT incorporates a
321 snow model based on the CROCUS snowpack model [Brun *et al.*, 1992]. MAR has been
322 validated through comparison with ground measurements [e.g. Lefebre *et al.*, 2003; Gallée
323 *et al.*, 2005; Lefebre *et al.*, 2005], satellite data [e.g. Fettweis *et al.*, 2005, 2011; Tedesco *et*
324 *al.*, 2011, Alexander *et al.*, 2014], and applied to simulate long-term changes in the GrIS
325 SMB and surface melt extent [Fettweis *et al.*, 2005, 2011; Tedesco *et al.*, 2008, 2011;
326 Tedesco and Fettweis, 2012]. Data are freely available from an online repository [Tedesco
327 *et al.*, 2015].

328 Meltwater production was used for grid cells classified by MAR as greater than 99%
329 ice sheet to mask the tundra region of Greenland. In addition, meltwater production values
330 of less than 1 mm day⁻¹ in all grid cells were recoded to zero to account for MAR’s scaled
331 output. This threshold could be considered a conservative approximation of the occurrence
332 of surface melt [Fettweis *et al.*, 2011, Figure 2]. Finally, grid cells were masked in the
333 interior ice sheet where mean monthly meltwater production does not exceed 1 mm day⁻¹ to
334 account for spurious correlations arising from a very limited number of dates that result in
335 nonzero mean monthly values of meltwater production.

336 Trends for each pixel (or regional averages) are only computed if at least 30 years of valid
337 data are found at that pixel. This ensures statistics are not biased by changes in spatial extent of
338 the sea ice or Greenland melt. However, Greenland melt has been observed to extend to higher
339 elevations in recent years, and in 2012 nearly the entire ice sheet experienced melt events [e.g.
340 Nghiem *et al.*, 2012]. Regional means are area-weighted. Trends are computed using linear-
341 least squares and statistical significance is evaluated with a student T-test at the 95 and 99%
342 levels.

Deleted: .

343 **2.2 Atmospheric Data**

344 Geopotential heights at 500 hPa and hourly 10 m wind speeds were obtained from
345 NASA’s Modern Era Retrospective-Analysis for Research and Applications (MERRA)
346 products [Bosilovich *et al.*, 2011; Cullather and Bosilovich, 2011a, 2011b; Rienecker *et al.*,
347 2011]. MERRA is run on a 1/2° latitude by 2/3° longitude global grid with 72 hybrid-sigma
348 vertical levels to produce analyses from 1979 to present. MERRA has been evaluated
349 extensively since its release [Cullather and Bosilovich, 2011b; Kennedy *et al.*, 2011;
350 Reichle *et al.*, 2011] and has compared favorably with other reanalysis products in the
351 Arctic [Zib *et al.*, 2012; Cullather and Bosilovich, 2011; Lindsay *et al.*, 2014].

352 We also utilize atmospheric variables from NASA’s Atmospheric Infrared Sounder
353 (AIRS), designed specifically to map atmospheric water vapor content. This instrument has

355 been used in several recent studies to document atmospheric changes and impacts on sea
356 ice in the Arctic [e.g. *Boisvert and Stroeve, 2015; Stroeve et al., 2014; Serreze et al., 2016*].
357 While the data record is rather short (begins in September 2002), it provides twice daily
358 global coverage at 1-degree spatial resolution of several key atmospheric variables,
359 including skin and air temperature, precipitable water, cloud fraction and specific humidity.
360 In this study we utilize the Level 3 Version 6 skin temperatures, 1000 hPa air temperature,
361 effective cloud fraction, near surface specific humidity and total precipitable water.
362 Additional variables derived from AIRS data products include the moisture flux [*Boisvert*
363 *et al., 2013; 2015*], turbulent sensible heat flux and downwelling longwave radiation
364 [*Boisvert et al., 2016*].

365 **3. Methods**

366 **3.1. Region of Interest and Study periods**

367 For local assessment of sea ice changes and corresponding ice sheet changes, we define 5
368 sea ice and 5 adjacent ice sheet regions. Since we are examining the potential influence of the
369 ocean on the ice sheet, it makes sense for the ocean regions selected to define the ice sheet
370 boundaries, rather than the other way around. The definition of the sea ice boundaries comes
371 from the International Hydrographic Organization, and we define 5 sea ice regions: Baffin Bay,
372 David Strait, Lincoln Sea, Greenland Sea and the North Atlantic together with associated
373 Greenland regions [Figure 2]. For the ice sheet, each region is defined along a topographical
374 divide. While there are many local topographical divides, only those regions that matched the
375 ocean delineations were selected.

376 We use two study periods. First, we do analysis from 1979 to 2015 when analyzing sea ice,
377 melt extent and MAR model outputs. Second, AIRS data analysis is applied from 2003 to 2015
378 since a full year of data collection did not begin until 2003.

Deleted: n't

379 **3.2 Relationship between SIC and GrIS melt**

380 To investigate covariability between summer SIC, GrIS melt water production, and 500
381 hPa geopotential heights, singular value decomposition (SVD) was applied to two fields at
382 a time to produce pairs of coupled spatial patterns that explain their maximum mean
383 squared temporal covariance [Bretherton *et al.*, 1992]. The advantage of SVD is that it is
384 able to maximize the covariance between the two fields to explicitly show the structure of
385 the covariability.

386 The temporal evolution of each pair's corresponding pattern in the two datasets is
387 represented by the pair's associated expansion coefficients (EC), where subscripts GrIS,
388 SIC and 500 denote the EC for ice sheet melt, sea ice concentration, and 500 hPa heights,
389 respectively. These ECs were used to calculate heterogeneous correlation (HC) maps,
390 which show the correlation coefficients between each EC and the opposing data field. The
391 normalized squared covariance (NSC) associated with each pair of spatial patterns
392 indicates the total strength of this relationship [Wallace *et al.* 1993], with values greater
393 than approximately 0.10 considered to indicate a significant relationship [Riaz *et al.* 2017].

Deleted: ..

Formatted: Font:Italic

Formatted: Font:Italic

394 SVD has widely been used to investigate coupled modes of variability, including
395 relationships between Arctic sea ice and snow cover [Ghatak *et al.*, 2010], and Arctic sea
396 ice and atmospheric variables [Stroeve *et al.*, 2008].

397 To further investigate how SIC in these regions is related to GrIS melt, SIC for both
398 regions was spatially aggregated, de-trended and correlated with de-trended time series of
399 GrIS meltwater production and the Greenland Blocking Index (GBI), respectively [NOAA,

402 The GBI is defined as the 500 hPa geopotential height field averaged between 20° –
403 80° W, 60° – 80° N [Fang, 2004; Hanna *et al.*, 2013], and is used as a metric for large-
404 scale atmospheric circulation patterns over Greenland. To remove the influence of the GBI
405 on both SIC and GrIS melt, we performed a partial correlation analysis of SIC in each
406 region and GrIS meltwater production after the trends in GBI were removed [e.g. Cohen *et*
407 *al.*, 2003].

408 **3.3 Energy Balance**

409 Following Koenig *et al.* [2014], the net heat flux into the atmosphere (F_{net}) emitted
410 from the ocean is defined by:

$$411 \quad F_{net} = Q_h + Q_e + LW - SW \quad (1)$$

412 where SW is the downward shortwave radiative flux at the surface, LW is the net upward
413 longwave radiation, Q_h is the sensible heat flux, or heat transferred from the surface to the
414 atmosphere by turbulent motion and dry convection, and Q_e is the latent heat flux, or heat
415 extracted from the surface by evaporation. If the sum of the four right-hand side terms is
416 positive, there is a net flow of heat from the surface to the atmosphere and vice versa.
417

418 Previous studies have looked at the strong seasonality in F_{net} over the Arctic Ocean
419 [e.g. Serreze *et al.*, 2007], with strong downward fluxes in summer and large upward fluxes
420 in January associated with heat gain and loss, respectively, in the subsurface column.
421 Updated trends from NCEP/NCAR reanalysis confirm that F_{net} trends are small in winter
422 (January to April), except in the Barents Sea as a result of reduced sea ice and increased
423 oceanic heat flux [Ornheim *et al.*, 2016] and also within Baffin Bay, again a result of less
424 winter ice cover. Thus, in these two regions there is a transfer of heat from the ocean to the
425 atmosphere during the winter months, which may spread over the sea ice areas and limit
426 winter ice growth. In summer however (May to August), the direction is generally reversed
427 with large heat fluxes from the atmosphere going towards the surface.

428 In this study we focus on how early sea ice retreat, as indicated by early melt onset
429 during the transition from winter to summer, impacts the heat and moisture fluxes over
430 early formed open water areas, and whether or not this is sufficient to impact Greenland
431 melt. Towards this end, we composite the turbulent fluxes in Eq. 1 for low and high sea ice
432 years, specific to each individual region analyzed using the AIRS data, with positive fluxes
433 showing energy transfer from the surface to the atmosphere. We use the criteria of
434 anomalies in melt onset exceeding 1 standard deviation (1σ) for each region when
435 compositing. All data are detrended by subtracting the linear trend before computing the
436 composites.

437 **4. Results**

438 We begin with an assessment of the large-scale relationship between SIC and
439 Greenland melt and its spatial covariability (4.1). This is followed by an analysis of
440 changes in the sea ice cover surrounding Greenland, both in terms of SIC and OWF (4.2),
441 followed by analysis of the timing of sea ice MO onset and FO, and its relationship with
442 Greenland MO (4.3). Finally, turbulent heat and moisture flux changes composited for
443 early and late melt onset years are examined (4.4) and large-scale influences are examined
444 in section 4.5.

Deleted: 2

Deleted:

447 **4.1 Relationship between Sea Ice and Greenland Melt**

448 The leading SVD mode explains the majority of the mean spatial covariance between
449 monthly GrIS meltwater production and SIC in June and July (62%, 73%, respectively) and
450 less than half (42%) in August. However, NSC values of 0.099 in June and only 0.081 and
451 0.066 in July and August, respectively, provide weak overall support for a significant
452 relationship between SIC and GrIS meltwater production. HC maps reveal opposing sign of
453 the correlations between the map pairs [Figure 3: columns 1 and 2; and columns 3 and 4]
454 indicating an anticorrelation, meaning that increased ice sheet melt extent covaries with
455 decreased sea ice area (it is irrelevant in the HC maps which is positive and which is
456 negative). Specifically, the covariability of GrIS meltwater production and SIC, expressed as
457 correlations on an HC map, show that sea ice and ice sheet melt strongly covary in two
458 general regions, namely Baffin Bay/Davis Strait in June, and a large part of Beaufort Sea in
459 June and July [Figure 3(a) and (e)]. In June, SIC in both the Baffin Bay/Davis Strait and
460 the Beaufort Sea regions have strong correlations with EC_{GrIS} , $|r| > 0.70$, and GrIS
461 meltwater production is highly correlated with EC_{SIC} for the majority of the unmasked ice
462 sheet surface [Figure 3b]. The strong correlation in the Beaufort Sea persists in July but
463 not in Baffin Bay/Davis Strait, and neither exhibits a significant correlation in August
464 [Figure 3(e) and (i)]. At the same time, GrIS meltwater production correlations with EC_{SIC}
465 are less expansive over the ice sheet in July and August, particularly in southern Greenland
466 [Figure 3(f) and (j)].

Deleted: ,

Deleted: and (i)

467 In the second SVD analysis of 500 hPa geopotential heights and GrIS melt water
468 production, the leading SVD mode explains the majority of mean spatial covariance of the
469 two variables in June and July (79% and 60%, respectively), but less than half in August
470 (37%), which are similar values to the leading SVD mode for GrIS melt and SIC [Figure
471 3(c), (g) and (k)]. An NSC value of 0.191 indicates a significant relationship between GrIS
472 melt and SIC in June, with more of a marginally significant relationship in July and August
473 given NSC values of 0.111 and 0.093, respectively. The HC maps show a strong tendency
474 for positive height anomalies centered on the Greenland side of the Arctic, though this area
475 shrinks in July and August [Figure 3(c), (g) and (k)]. As before, this spatial pattern
476 covaries with GrIS melt water production over most of the ice sheet in June, but is
477 somewhat more restricted in extent in July and August. While SIC and GrIS melt extent
478 covary regionally, large parts of the same areas of the GrIS melt extent region also covary
479 with 500 hPa geopotential height fields. The similar spatial patterns in GrIS melt
480 covariability with SIC and 500 hPa geopotential height fields suggest that the large-scale
481 circulation may be a dominant explanation for the SIC – GrIS melt covariability. Before this
482 possibility is examined more closely, we analyze trends in SIC and GrIS melt patterns and
483 timing.

Deleted: P

Deleted: A

484 **4.2 Changes in the Sea Ice Cover around Greenland**

485 The above analysis suggests a local-scale influence from SIC on GrIS melt within
486 Baffin Bay and Davis Strait during June. This region of high SIC-GrIS covariability has
487 experienced a sharp drop in SIC since 1979 [Figure 4]. In Baffin Bay and Davis Strait, SIC
488 trends are negative in all seasons, and are particularly large in winter (DJF), spring (MAM)
489 and summer (JJA) [Figure 4a-d]. In contrast, SIC trends in the East Greenland Sea are
490 mixed, which may in part explain the lack of covariability within this region. Adjacent to
491 the Greenland's east coast, positive SIC trends occur throughout winter and spring. Further
492 east, reductions in SIC are confined to the area where the Odden used to form (c.f. Figure

497 2). During summer and fall, negative SIC anomalies persist along eastern GrIS, though
498 they remain smaller than on the western side. North in the Lincoln Sea region, there is
499 essentially no change in SIC year-round except for slight negative trends in summer.

500 Negative SIC trends have resulted in longer open water periods surrounding Greenland
501 [**Figure 4e**]. Trends in annual open water days are mostly positive everywhere, the
502 exceptions being the Lincoln Sea, which remains ice-covered year around, and the southern
503 part of Davis Strait towards the Labrador Sea, a region where ice has expanded during
504 recent winters. In some locations within Baffin Bay and the East Greenland Sea the number
505 of open water days has increased by as much as 30 to 40 days per decade, but regionally
506 averaged trends are generally on the order of 2 weeks per decade.

507 The strength of the OWF trends and exact timing of when these trends peak around the
508 GrIS reveal large spatial differences [**Figure 5**]. The largest OWF trends occur in Baffin
509 Bay during week 26 (third week of June), and are on the order of $10\% \text{ dec}^{-1}$, with a
510 secondary peak during week 44 (end of October). Further south in Davis Strait, OWF are
511 positive throughout winter and into July ($\sim 5\% \text{ dec}^{-1}$), reflecting both earlier ice retreat and
512 later winter ice formation, with the largest trends during week 52 ($6\% \text{ dec}^{-1}$). East of
513 Greenland, positive OWF trends are found throughout the year in the Greenland Sea, but
514 are considerably weaker than found in Baffin Bay and Davis Strait. Finally, Lincoln Sea
515 OWF trends are mostly negative (except in June and August), though trends are generally
516 less than $1\% \text{ dec}^{-1}$, and are not statistically significant. For comparison the Arctic Ocean
517 OWF trends are also shown, showing peak OWF trends around week 38 (mid-September),
518 reflecting the timing of the pan-Arctic sea ice minimum.

519 **4.3 Changes in the Melt Season**

520 We next examine if there is a link between the timing of EMO, MO, and FO over sea
521 ice and over GrIS. The link between MO and the timing of ice retreat has already been
522 established, with correlations between the detrended melt onset and detrended ice retreat
523 dates greater than 0.4 [See Figure S10, Stroeve *et al.*, 2016].

524 Climatological regional mean values of EMO, MO, FO show that melt begins earlier
525 and freeze-up happens later over the sea ice than it does on the ice sheet, and can be largely
526 explained by temperature dependencies on elevation [**Table 1**]. In western Greenland, the
527 continuous MO period for sea ice begins about 9 days earlier than on the ice sheet in the
528 Baffin Bay region, and 15 days earlier in the Davis Strait region, whereas ice sheet FO
529 occurs on average in early to mid-September, compared to the end of October (Baffin Bay)
530 to the end of November (Davis Strait) over the adjacent sea ice. Similarly, in the Greenland
531 Sea region, MO begins around 20 days earlier over the sea ice than on the ice sheet and FO
532 happens about a month later. In contrast, the Lincoln Sea region exhibits similar timing in
533 both MO and FO, which may be explained by the fact that this is the smallest region, and
534 also the region furthest north where most melting will only occur at lowest GrIS elevations.
535 Since there is little sea ice in the North Atlantic (e.g. regionally the open water season lasts
536 for 360 days), MO and FO dates are not meaningful, but generally show values similar to
537 as that observed in Davis Strait.

538 EMO, MO and FO trends for SIC and GrIS are of the same sign, indicating an overall
539 lengthening of the melt season over the last 37 years in both environments [**Figure 6**].
540 Baffin Bay experiences the largest trends towards earlier MO and later FO, with regionally
541 averaged trends of -8.3 and $+7.8 \text{ days dec}^{-1}$, respectively, statistically significant at 99%
542 confidence [**Table 2**]. This has led to an increase in the melt season length on the order of
543 16 days per decade. GrIS trends in the same region are typically smaller, especially in

544 regards to the timing of freeze-up ($4.6 \text{ days dec}^{-1}$) and melt season duration ($11.1 \text{ days dec}^{-1}$). In contrast, larger statistically significant trends in both MO and FO are seen over the
545 Davis Strait GrIS region, leading to a lengthening of the melt season that is larger than over
546 the adjacent sea ice ($18.7 \text{ days dec}^{-1}$ compared $11.7 \text{ days dec}^{-1}$).
547

548 On Greenland's eastern side, similar ice sheet/sea ice MO trends are observed, but sea
549 ice FO trends are smaller, and not statistically significant. The exception is the North
550 Atlantic region, which exhibits large positive FO trends of $8.9 \text{ days dec}^{-1}$, resulting in an
551 overall increase in melt season duration of $16.3 \text{ days dec}^{-1}$. However, given the low
552 frequency of sea ice in this region, caution is warranted when interpreting these trends
553 since ocean dynamics play a large role in the year-to-year variability in these values.
554 Nevertheless, the largest trends in melt season duration over the eastern GrIS are also
555 found in the North Atlantic sector ($22.1 \text{ days dec}^{-1}$), primarily a result of earlier MO. The
556 Greenland Sea GrIS sector also exhibits large trends in melt duration ($14.4 \text{ days dec}^{-1}$), but
557 earlier MO and later FO play a nearly equal role here. Interestingly, the Lincoln Sea GrIS
558 region also displays large trends in melt season duration ($12.7 \text{ days dec}^{-1}$), considerably
559 larger than seen over the adjacent sea ice ($5.5 \text{ days dec}^{-1}$). While the climatological mean
560 timing of MO and FO is broadly similar over both the sea ice and the GrIS in the Lincoln
561 Sea GrIS region, there has been a trend towards much later freeze-up ($6.8 \text{ days dec}^{-1}$).
562

563 Finally, we examine whether there is synchronicity in the timing of melt onset and
564 freeze-up between the sea ice and the ice sheet. In the Baffin Bay sector, the correlations
565 between the sea ice and ice sheet MO and FO (respectively) exceed $0.6; p=0.001$. High
566 correlations ($r>0.6$) are also seen in the Lincoln Sea sector and for EMO in the Greenland
567 Sea sector ($r=0.6; p=0.001$). Correlations are reduced when MO, FO and EMO records are
568 detrended, yet remain significant in the Baffin Bay and Lincoln Sea regions: detrended
569 correlations for sea ice and the ice sheet EMO, FO and melt season duration exceed $r=0.5,$
570 $p=0.001$ in Baffin Bay as well as the Lincoln Sea in regards to the MO, $p=0.002$. Elsewhere, no significant relationship is found.

571 **4.4 Impact of sea ice changes on surface energy fluxes**

572 Next we examine the relationship between early and late MO and variations in
573 atmospheric moisture and heat fluxes using lag-correlation and composites for early and
574 late MO years. We begin with an assessment of the differences in the strength of turbulent
575 fluxes between early and late MO years. All months are shown to allow for both an
576 assessment of what drives early MO over sea ice as well as to determine how early sea ice
577 MO influences the overlying atmosphere [Figure 7].

578 On average, the transfer of latent heat flux occurs from the ocean to the atmosphere
579 year-round in all regions, except the Lincoln Sea in Sep-May, and Baffin Bay in Dec-Feb.
580 In Baffin Bay and Lincoln Sea, latent heat flux transferred to the atmosphere is small until
581 the sea ice begins to break up and melt in the summer and moisture is released from the
582 previously ice-covered ocean. Latent heat fluxes are directed into the atmosphere year-
583 round in Davis Strait and Greenland Sea due to large areas of ice-free ocean that persists
584 throughout the year.

585 Sensible heat flux is generally directed towards the surface for regions that are 100%
586 sea ice covered during the cold season months (e.g. Baffin Bay and the Lincoln Sea) and
587 then switches towards the atmosphere as the sea ice retreats in summer (Baffin Bay only).
588 Regions that have large fractions of open water year-round generally have a net sensible
589 heat flux transfer towards the atmosphere year-round, though some exceptions occur.
590 Greenland Sea and Davis Strait exhibit sensible heat flux to the atmosphere in early spring

591 and late fall (October-December) when the ice-free ocean surface is much warmer than the
592 overlying air; due to the higher heat capacity of water, the opposite is true for ice-covered
593 regions.

594 A larger amount of sensible and latent heat flux tends to enter the atmosphere in the
595 spring during early MO years in all regions. However, the Baffin Bay region is the only
596 region with a majority of positive fluxes throughout the year. When melt happens early in
597 Baffin Bay, the additional sensible and latent heat fluxes result in $\sim 14 \text{ W m}^{-2}$ entering the
598 atmosphere in spring (March-June) and $\sim 25 \text{ W m}^{-2}$ in autumn (September-December) due
599 to a later FO. In contrast to Baffin Bay, turbulent flux anomalies in early MO years from
600 Davis Strait and Lincoln Sea show no strong consistent pattern and switch between positive
601 anomalies throughout the year. Compared to Baffin Bay, Davis Strait, which is further
602 south, has larger latent heat fluxes entering the atmosphere between February-August
603 during years with earlier MO, whereas sensible heat flux into the atmosphere is only larger
604 during early MO years in February, April and November, reflecting both early MO (April)
605 and later FO (November). Over the Lincoln Sea there are no fluxes of heat or moisture into
606 the atmosphere during the late fall, winter and early spring due to the solid sea ice pack.
607 However, by June there is an additional $\sim 12 \text{ W m}^{-2}$ of turbulent flux energy transferred to
608 the atmosphere during early melt years. This generates smaller turbulent fluxes in July due
609 to warmer air temperatures than when melting has just begun in late MO years. The early
610 MO year turbulent flux anomalies from Greenland Sea are different from the other three
611 regions, as there is more heat and moisture entering the atmosphere in January, March,
612 October and December during early MO years.

613 Sensible and latent heat fluxes transfer heat and moisture into the local atmosphere and
614 can cause the temperature and humidity to increase, which in turn should produce larger
615 downwelling longwave flux at the surface due to the greenhouse feedback effect. Thus one
616 would expect to see a larger net longwave flux (downwelling – upwelling) at the surface
617 during early MO years when the local atmosphere contains more heat and moisture. We see
618 evidence of this occurring until roughly July as there is more net longwave directed
619 towards the surface of the ice sheet in most regions when the sea ice melts earlier [Figure
620 8]. In August the surface net longwave flux turns largely negative during early MO years,
621 partly because the warmer ice sheet results in dominance of upwelling radiation fluxes, and
622 partly because there is less of an influence of early season conditions.

623 The increase in heat and moisture into the atmosphere from the surrounding ocean in
624 early MO versus late MO years and subsequent increase in energy at the ice sheet surface is
625 shown in more detail for Baffin Bay in Figures 9(a) and (d). In April and May (day 1 to 61
626 in Figure 9), there appears to be an out-of-phase relationship between latent heat flux over
627 Baffin Bay and the specific humidity over the adjacent ice sheet, with pulses of moisture
628 coming from the ocean surface being followed about a week later with rising specific
629 humidity over the ice sheet. A similar pattern is observed between ocean sensible heat flux
630 and near surface air temperature over GrIS. In June and July (day 61 to 92), latent and
631 sensible heat flux anomalies for early/late MO years fluctuate around zero, which suggests
632 these fluxes are similar between early and late MO years. In contrast, the specific humidity
633 and temperature are higher in late MO years over the ice sheet in July (negative anomalies
634 in Figure 9a and 9d). This could be due to a roughly one-month delay in late MO years
635 compared to early MO for the sea ice, which causes increases in the temperatures and
636 humidity later in the season (July) over the ice sheet. From the timing of early sea ice MO
637 (dotted blue line) to early GrIS MO (dotted blue, highlighted red line), large fluxes of

Deleted: b

Deleted: 9b

Deleted: 9a
Formatted: Font:Bold
Deleted: top

Deleted: 9b
Formatted: Font:Bold

moisture and heat released via the latent and sensible heat flux from the ice/ocean surface precede elevated humidity and temperature over the ice sheet.

One-week running lagged correlations between latent heat flux from the ocean and specific humidity over the ice sheet show large positive correlations during early MO years [Figure 9b, solid blue lines], suggesting increased evaporation from earlier MO over sea ice may be driving the observed increase in specific humidity over the ice sheet one week later. A one-week lag was chosen because sea ice and GrIS MO in Baffin Bay occur about 9 days apart on average, and also because water vapor in the troposphere has a residence time of about two weeks. These three highly correlated events precondition the ice sheet for earlier MO by increasing the specific humidity and thus the downwelling longwave flux earlier in the spring. In late MO years, the sea ice/ocean does also appear to play a small role in initiating MO on the ice sheet. Large amounts of latent heat are released from the surface in Baffin Bay at the timing of late MO, which in turn is correlated to increases in specific humidity over the ice sheet directly before MO, initiating melt (solid green lines). Since Baffin Bay MO is much later (~1 month) in late melt years, excess moisture into the atmosphere is delayed. Though because the environment is already warming seasonally, it does not require extra preconditioning for the melt to begin on GrIS compared to early melt years. This case is very similar to sensible heat flux released from Baffin Bay and ensuing temperature over the ice sheet [Figure 9c]. Comparing these 1-week lagged correlations to a zero-lag correlation (not shown), correlations for all variables in early and late MO years are highly negative, meaning they are out of phase [Figure 9d].

Note also there are instances in April when both early and late melt years exhibit high correlations between either sensible or latent heat from the sea ice region and specific humidity or temperature over GrIS one week later. This may be related to opening of the North Water Polynya [Boisvert et al., 2012]. As the open ocean is relatively warm compared to the overlying air in April, heat and moisture fluxes enter the atmosphere and are subsequently transferred over the ice sheet, increasing the specific humidity and air temperature.

In summary, sea ice in Baffin Bay/Davis Strait and the adjacent ice sheet surface conditions appear connected. MO and breakup of the sea ice triggers enhanced flux of heat and moisture into the atmosphere, which are observed over the ice sheet within a week. This results in a warming and moistening the local environment and preconditions the ice sheet for melt in early MO years. Therefore, when the MO of the sea ice is earlier, MO of GrIS is earlier and vice versa.

674 **4.5 Influence of large scale atmospheric variability on Baffin Bay 675 and Beaufort Sea**

676 The SVD analysis (4.1) indicated that both Baffin Bay/Davis Strait and the Beaufort
677 Sea are regions with SIC and GrIS melt water production covariability. In the case of
678 Baffin Bay/Davis Strait, this was supported by the melt and turbulent heat flux analysis.
679 Next we examine the influence of the large-scale atmospheric variability on this
680 covariability using Pearson correlation and partial correlation.

681 In the Beaufort Sea, both 500 hPa heights and SIC closely covary, particularly in June
682 [Figure 10a], in concert with high SIC covariance in this region with EC_{GrIS} in the HC
683 maps [Figure 3]. Here, the positive correlations between SIC and GrIS melt weaken
684 significantly after June with almost no correlation by August [Table 3]. The strong
685 relationship between Beaufort SIC and GrIS melt in June is reduced considerably when the

689 GBI index is removed via partial correlation, as significant correlations remain only in
690 southeast Greenland.

691 The correlation between SIC in Baffin Bay/Davis Strait and geopotential heights is
692 relatively strong but not as extensive in June, while this signal mostly disappears in July
693 and especially August [Figure 10d; Table 3]. This is associated with a weakening Baffin
694 Bay SIC correlation with EC_{GrIS} in the HC maps [Figure 3(a), (e) and (i)]. Statistically
695 significant correlations with meltwater production are focused on the west side of the ice
696 sheet in June [Figure 10e], but are minimal in July and August when correlations over only
697 7% and 2% of the respective unmasked ice sheet area are statistically significant. Partial
698 correlation analysis indicates that the GBI explains approximately two thirds of this
699 correlation in each month, though this still leaves the possibility that variations in Baffin
700 Bay sea ice are in part responsible for the correlation with surface melt in western
701 Greenland.

702 Because there is a potential local influence from Baffin Bay and Davis Strait, we next
703 focus on GrIS melt only in west-central Greenland. The highest and lowest melt years in
704 west-central Greenland (after removing trends) consistently correspond to patterns of
705 anomalous SIC and geopotential heights in these years [Figure 11]. These variables show
706 much less variation by month, though a weaker relationship appears particularly in the
707 height field, which follows results from the SVD analysis [Figure 11 (g)-(l)]. Additionally,
708 a strong SIC pattern is evident not just in western Greenland but consistently on the east
709 side of Greenland that is equally as strong [Figure 11(a)-(f)]. This suggests that the
710 processes responsible for this signal expression to the west of Greenland probably also
711 exist on a large enough scale to have an effect of similar strength on sea ice off
712 Greenland's east coast; most likely a persistent ridge or trough, as suggested by the above
713 results. By August, sea ice in Baffin Bay has melted in most years, but positive anomalies
714 in SIC still appear in the lowest Greenland melt years [Figure 11(f)].

715 In summary, the SVD analysis suggest covariability between SIC and GrIS melt in the
716 Baffin Bay region (Fig. 3) that cannot fully be explained by large scale atmospheric
717 patterns (Fig 10 and 11). Examination of a set of hypotheses applied for the entire GrIS and
718 surrounding seas shows that trends and patterns in the Baffin and Davis Strait regions are
719 consistent with local scale influence [Table 4]. In contrast, no other regions have evidence
720 of covariability or trends and patterns consistent with local scale influence.

721 5. Discussion

722 Sea ice and Greenland ice sheet melt demonstrate localized covariability during the
723 summer, particularly June. While the majority of this relationship appears related to
724 simultaneous atmospheric circulation forcing, analysis over Baffin Bay/Davis Strait and the
725 adjacent ice sheet indicates that the covariability may additionally include a local-scale
726 influence. This is in agreement with previous work by *Rennermalm et al. [2009]* who found
727 the SIE and GrIS surface melt extent to co-vary in the western part of the ice sheet, though
728 the strongest relationships were found in August rather than June. Part of the discrepancy
729 might be explained by the study period. This study extends through 2015 and includes
730 years with larger anomalies in both SIC and GrIS melt. However, June is the time of year
731 with the largest trends in OWF, reflecting earlier development of open water at a time
732 when the atmosphere is still relatively cold. Thus, it is not surprising that we find stronger
733 covariability in June and a link with melt onset. An additional area of covariability in terms
734 of melt onset timing is also seen in the Lincoln Sea sector.

Deleted: significant

736 While statistical analysis suggests a local-scale influence may be present on the western
737 side of the ice sheet, the ability for the sea ice to influence GrIS melt depends on having
738 anomalous heat and moisture sources that can travel to the ice sheet. In this study we find
739 that turbulent fluxes are often larger during early MO years in the spring and fall because
740 areas where the ocean is ice-free tends to be warmer than that of the air, due to the higher
741 heat capacity of water. Both latent and sensible heat fluxes are larger and more positive
742 (from the ocean surface to the atmosphere) during early MO years, resulting in increased
743 air temperature and specific humidity especially in May when the atmosphere is ~2 K
744 warmer and $\sim 0.5 \text{ g kg}^{-1}$ wetter. This excess heat and humidity increases downwelling
745 fluxes to the ice sheet earlier in the year, preconditioning the ice sheet and triggering melt
746 (also shown in Figure 8). For late MO years, this phenomenon occurs later in the season,
747 and this is most likely why we see larger fluxes during late MO years in the summer
748 months (i.e. July depending on the climatology of the region). This is specifically true for
749 Baffin Bay, where throughout the winter months the region is completely covered by sea
750 ice, creating a barrier between ocean-atmosphere energy exchanges. This is also valid for
751 the Lincoln Sea in the context of melt ponds and a higher occurrence of leads forming on
752 the thick multi-year ice during the summer months.

Deleted: this phenomena

753 Turbulent fluxes from increased open water can reach well above the boundary layer
754 [e.g. Yulaeva *et al.*, 2001], but this depends on the frequency of spring and early summer
755 inversions that cap the atmospheric boundary layer. Furthermore, if katabatic winds are
756 persistent at the ice edge, this will keep onshore flow from reaching the ice sheet [Noël *et*
757 *al.*, 2014], though a possibility remains for mixing in the boundary layer via a barrier wind
758 mechanism [van den Broeke and Gallée, 1996]. Analysis of daily winds around the timing
759 of sea ice melt, show that during early MO years over the sea ice, wind direction is from
760 the open water areas of Baffin Bay onto the GrIS, which helps support our claims that
761 earlier melt onset in part drives early melt over Greenland [**Figure 12**]. In late MO years,
762 the wind direction is reversed.

763 Finally, we note that SVD analysis reveals the strongest relationship between GrIS melt
764 and sea ice variability occurs within the Beaufort Sea. This appears to be related to the
765 positioning of a ridge near Greenland that enhances both ice sheet melt and sea ice retreat
766 as stronger easterlies help to circulate ice west out of the Beaufort Sea. SVD analysis
767 shows the covariability in June is reduced considerably when the GBI index is removed via
768 partial correlation, evidenced by the large reduction in percentage of grid cells with a
769 significant correlation (not shown). This explanation is supported by the relatively weak
770 value of NSC for June GrIS melt and SIC, which nearly doubles to 0.191 in the SVD
771 analysis of 500 hPa geopotential heights instead of SIC. The Greenland blocking
772 mechanism has been identified previously as a way to transport and melt ice between the
773 Beaufort Sea and the East Siberian Sea [Rogers, 1978; Maslanik *et al.*, 1999]. We speculate
774 that no mechanism originating from sea ice variability directly influences GrIS melt from a
775 distance of hundreds of kilometers away, though Liu *et al.* (2016) argue that sea ice loss
776 within the central Arctic has favored stronger and more frequent blocking events over
777 Greenland.

Deleted: is

778 In 2012, as the sea ice cover reached its all-time record low September extent, the
779 Greenland ice sheet also experienced a record amount of surface melt and ice mass loss
780 [Tedesco *et al.*, 2013]. Several explanations have been put forth to explain this anomalous
781 melt, including increased downwelling longwave radiation from low-level liquid clouds
782 [Bennartz *et al.*, 2013], advection of moist warm air over Greenland [Neff *et al.*, 2014] and
783 dominance of non-radiative fluxes [Fausto *et al.*, 2016]. While this event was likely a result

786 of atmospheric circulation patterns that transported warm, humid air over the southern and
787 western part of the ice sheet, the sea ice melt season began a week earlier than the 1981-
788 2010 long-term mean over Davis Strait and 3 days earlier over Baffin Bay. This earlier
789 melt onset of the sea ice may have provided an additional source of warm, moist air over
790 the adjacent ice sheet.

791 **6. Conclusions**

792 Based on multiple lines of statistical evidence, we identified western Greenland as a
793 region where direct influence from sea ice on the GrIS SMB is possible. SVD analysis
794 revealed that extreme melt years over the adjacent ice sheet are accompanied by strong SIC
795 anomalies within Baffin Bay and Davis Strait that would be expected if a local-scale
796 thermodynamic influence were occurring. This is true even after near surface temperature
797 and climate index influences are removed.

798 The covariance is strongest in June, which may be partially due to the lower variability
799 in interannual June meltwater production over the entire ice sheet relative to the rest of
800 summer, with a standard deviation simulated by MAR of 0.84 mm water equivalent day⁻¹
801 compared to 0.95 in August and 1.12 in July. Additionally, June variability in sea ice may
802 have a greater potential to influence GrIS melt given that the ice sheet is transitioning into
803 its warm season regime and reaching the freezing point for the first time in many locations.
804 This is further confirmed through correlations between the timing of melt onset, which
805 occurs on average 9 days earlier over the sea ice than on the adjacent ice sheet, and in turn
806 allows for earlier development of open water and enhanced transfer of turbulent heat fluxes
807 from the ocean to the atmosphere. More heat and moisture is transported to the local
808 atmosphere from the ice-free ocean surface via turbulent fluxes in years when sea ice melts
809 earlier. Daily wind field analysis suggests these enhanced turbulent fluxes are transferred to
810 the ice sheet, allowing the local atmosphere over the GrIS to warm and become more
811 humid, which in turn impacts the net downwelling longwave flux, helping precondition the
812 surface for earlier melt onset.

813 However, despite evidence of a possible local-scale influence, all analysis incorporating
814 500 hPa height anomalies suggests that the large-scale atmospheric circulation remains the
815 primary melt driver in this part of the ice sheet as well as for the ice sheet as a whole.
816 Anomalous atmospheric circulation features include increased frequency of the negative
817 phase of the Arctic Dipole [Overland and Wang, 2010] and a persistently negative summer
818 North Atlantic Oscillation [van Angelen *et al.*, 2013]. Continued Arctic amplification and
819 associated shifts in Arctic atmospheric circulation and their persistence will theoretically
820 continue to enhance warming in the vicinity of Greenland [Francis and Vavrus, 2012,
821 2015]. Nevertheless, our study suggests a local response is also possible, and as the sea ice
822 cover continues to retreat around the Greenland ice sheet, this should present further
823 opportunities for local enhancement of summer ice sheet melt.

824 **Acknowledgements**

825 This work was funded by the National Science Foundation PLR 1304807. All data used in
826 this study were obtained from free and open data repositories. Detailed information is
827 provided in the methods section. The work of Linette Boisvert was funded from NASA
828 ROSES 2012 IDS proposal: 12-IDS12-0120. AIRS data are freely available at
829 www.airs.jpl.nasa.gov and MERRA2 data can be found at gmao.gsfc.nasa.gov.
830

831

832 **References**

- 833 Alexander, P. M., M. Tedesco, Z. Fettweis, R.S.W. van de Wal, C.J.P.P. Smeets and M.R.
 834 van den Broeke (2014), *The Cryosphere*, 8, 2293-2312, doi:10.5194/tc-8-2293-2014.
- 835 [Ballinger, T.J., E. Hanna, R.J. Hall and J.L. Hoyer \(2017\), Greenland coastal air](#)
 836 [temperatures linked to Baffin Bay and Greenland ice conditions during autumn through](#)
 837 [regional blocking patterns, *Clim. Dyn.*, doi:1007/s00382-017-3583-3.](#)
- 838 Bennartz, R., M.D. Shupe, D.D. Turner, V.P. Walden, K. Steffen, C.J. Cox, M.S. Kullie,
 839 N.B. Miller and C. Pettersen (2013), July 2012 Greenland melt extent enhanced by low-
 840 level liquid clouds. *Nature*, 496, 83–86, doi:10.1038/nature12002.
- 841 [Bezeau, P., M. Sharp and G. Gascon \(2014\), Variability in summer anticyclonic circulation](#)
 842 [over the Canadian Arctic Archipelago and west Greenland in the late 20th/early 21st](#)
 843 [centuries and its effect on glacier mass balance, *Int. J. Climatol.*, 35\(4\),](#)
 844 [doi:10.1002/joc.4000.](#)
- 845 Bhatt, U., D.A. Walker, M.K. Raynolds, J.C. Comiso, H.E. Epstein, G. Jia, R. Gens, J.E.
 846 Pinzon, C.J. Tucker, C.E. Tweedie, and P.J. Webber (2010), Circumpolar Arctic tundra
 847 vegetation change is linked to sea ice decline, *Earth Interactions*,
 848 doi:10.1175/2010E1315.1.
- 849 Boisvert, L. N., A. A. Petty, and J. C. Stroeve (2016), The impact of the extreme winter
 850 2015/2016 Arctic cyclone on the Barents-Kara seas, *Monthly Weather Review*,
 851 doi:10.1175/WMR-D-16-0234.
- 852 Boisvert, L. N., D. L. Wu, and C.-L. Shie (2015), Increasing evaporation amounts seen in
 853 the Arctic between 2003-2013 from AIRS data, *J. Geophys. Res. Atmos.*, 120, 6865-
 854 6881, doi:[10.1002/2015JD023258](#).
- 855 Boisvert, L.N. and J.C. Stroeve, (2015), The Arctic is becoming warmer and wetter as
 856 revealed by the Atmospheric Infrared Sounder, *Geophys. Res. Lett.*,
 857 doi:[10.1002/2015GL063775](#).
- 858 Boisvert, L. N., T. Markus, C. L. Parkinson, and T. Vihma (2012), Moisture fluxes derived
 859 from EOS Aqua satellite data for the North Water polynya over 2003-2009, *J. Geophys.*
 860 *Res.*, 117, D06119, doi:10.1029/2011JD016949.
- 861 Bosilovich, M. G., F. R. Robertson, and J. Chen (2011), Global Energy and Water Budgets
 862 in MERRA, *J. Clim.*, 24(22), 5721–5739, doi:10.1175/2011JCLI4175.1.
- 863 Bretherton, C.S., C. Smith and J.M. Wallace (1992), An intercomparison of methods for
 864 finding coupled patterns in climate data, *J. Climate*, 5, 451-560.
- 865 Brun, E., David, P., Sudul, M., and G. Brunot (1992), A numerical model to simulate
 866 snow-cover stratigraphy for operational avalanche forecasting. *J. Glaciol.*, 38(128), 13–
 867 22.
- 868 Cassano, E. N., J. J. Cassano, M. E. Higgins, and M. C. Serreze (2014), Atmospheric
 869 impacts of an Arctic sea ice minimum as seen in the Community Atmosphere Model,
 870 *Int. J. Climatol.*, 34(3), 766–779, doi:[10.1002/joc.3723](#).
- 871 Cavalieri, D., C. Parkinson, P. Gloersen, and H. J. Zwally (1996), updated 2008. Sea Ice
 872 Concentrations from Nimbus-7 SMMR and DMSP SSM/I Passive Microwave Data,
 873 [1979-2013]. Boulder, Colorado USA: National Snow and Ice Data Center. Digital
 874 media.
- 875 Cohen, J., P. Cohen, S. G. West, and L. S. Aiken (2003). *Applied multiple*
 876 *regression/correlation analysis for the behavioral sciences* (3rd ed.). Routledge,
 877 Mahwah.
- 878 Comiso, J.C., (2002), Correlation and trend studies of the sea-ice cover and surface
 879 temperatures in the Arctic, *Annals of Glaciology*, 34(1), pp.420–428.

Formatted: Font:Italic**Formatted:** Superscript**Formatted:** Superscript**Formatted:** Font:Italic**Deleted:** <http://www.nature.com/doifinder/10.1038/nature12002> (Accessed April 3, 2013).

Deleted: q

Formatted: Font:Italic

- 882 Cullather, R. I., and M. G. Bosilovich (2011a), The Energy Budget of the Polar
883 Atmosphere in MERRA, *J. Clim.*, 25(1), 5–24, doi:10.1175/2011JCLI4138.1.
884 Cullather, R. I., and M. G. Bosilovich (2011b), The Moisture Budget of the Polar
885 Atmosphere in MERRA, *J. Clim.*, 24(11), 2861–2879, doi:10.1175/2010JCLI4090.1.
886 Dee, D.P. and S. Uppala (2009), Variational bias correlation of satellite radiance data in the
887 ERA-Interim reanalysis, *Q. J. R. Meteorol. Soc.*, 135, 1830,1841, doi:10.1002/qj.493.
888 De Ridder, K., and H. Gallée (1998), Land surface-induced regional climate change in
889 southern Israel, *J. Appl. Meteorol.*, 37(11), 1470-1485.
890 Deser, C., J. E. Walsh, and M. S. Timlin (2000), Arctic Sea Ice Variability in the Context
891 of Recent Atmospheric Circulation Trends, *J. Clim.*, 13, 617–633.
892 Doyle, S. H., and Coauthors, (2015), Amplified melt and flow of the Greenland ice sheet
893 driven by late-summer cyclonic rainfall, *Nat. Geosci.*, 8, 647–653,
894 doi:10.1038/ngeo2482. <http://www.nature.com/doifinder/10.1038/ngeo2482>.
895 Enderlin, E.M., I.M. Howat, S. jeong, M-J. Noh, J.H. van Angelen and M.R. van den
896 Broeke (2014), An improved mass budget for the Greenland ice sheet, *Geophys. Res.
897 Lett.*, 41, doi:10.1002/2013GL059010.
898 Fang Z-F (2004), Statistical relationship between the northern hemisphere sea ice and
899 atmospheric circulation during wintertime. In: Observation, Theory and Modeling of
900 Atmospheric Variability. World Scientific Series on Meteorology of East Asia, Zhu X
901 (ed), World Scientific.
902 Fausto, R.S., D. van As, J.E. Box, I. Colgan, P.L. Langen and R.H. Mottram, (2016), The
903 implication of nonradiative fluxes dominating Greenland ice sheet exceptional ablation
904 area surface melt in 2012, *Geophys. Res. Lett.*, 43, doi:10.1002/2016GL067720.
905 Fettweis, X., Gallée, H., Lefebvre, F., and J.-P. van Ypersele, (2005), Greenland surface
906 mass balance simulated by a regional climate model and comparison with satellite-
907 derived data in 1990-1991. *Clim. Dyn.*, 24(6), 623-640. doi:10.1007/s00382-005-0010-
908 y.
909 Fettweis, X., M. Tedesco, M. van den Broeke, and J. Ettema (2011), Melting trends over
910 the Greenland ice sheet (1958–2009) from spaceborne microwave data and regional
911 climate models, *The Cryosphere*, 5(2), 359–375, doi:10.5194/tc-5-359-2011.
912 Francis, J.A. and S.J. Vavrus (2012), Evidence linking Arctic amplification to extreme
913 weather in mid-latitudes, *Geophys. Res. Lett.*, 39(6), doi:10.1029/2012GL051000.
914 Francis, J. A., W. Chan, D. J. Leathers, J. R. Miller, and D. E. Veron (2009), Winter
915 Northern Hemisphere weather patterns remember summer Arctic sea-ice extent,
916 *Geophys. Res. Lett.*, 36(7), L07503, doi:10.1029/2009GL037274.
917 Fyke, J.G., M. Vizcaino, W. Lipscomb and S. Price (2014a), Future climate warming
918 increases Greenland ice sheet surface mass balance variability, *Geophys. Res. Lett.*, 41,
919 doi:10.1002/2013GL058172.
920 Fyke, J.G., M. Vizcaino and W.H. Lipscomb (2014b). The pattern of anthropogenic signal
921 emergence in Greenland Ice Sheet surface mass balance, *Geophys. Res. Lett.*, 41(16),
922 doi:10.1002/2014GL060735.
923 Gallée, H., and G. Schayes (1994), Development of a three-dimensional meso-γ primitive
924 equation model – katabatic winds simulation in the area of Terra-Nova Bay, Antarctica.
925 *Mon. Wea. Rev.*, 122(4), 671-685.
926 Gallée H., Peyaud V., and I. Goodwin (2005), Simulation of the net snow accumulation
927 along the Wilkes Land transect, Antarctica, with a regional climate model. *Ann.
928 Glaciol.*, 41,17-22.
929 Ghatak, D., A. Frei, G. Gong, J. Stroeve, and D. Robinson, (2010). On the emergence of an

- 931 Arctic amplification signal in terrestrial Arctic snow extent, *J. Geophys. Res.*, 115,
 932 D24105, doi:10.1029/2010JD014007.
- 933 Hanna, E., X. Fettweis, S.H. Mernild, J. Cappelen, M.H. Ribergaard, C.A. Shuman, K.
 934 Steffen, L. wood and T.L. Mote (2013), Atmospheric and oceanic climate forcing of the
 935 exceptional Greenland ice sheet surface melt in summer 2012. *Int. J. Climatol.*,
 936 doi:10.1002/joc.3743.
- 937 Hanna, E., et al. (2008), Increased runoff from melt from the Greenland ice sheet: A
 938 response to global warming, *J. Clim.*, 21, 331 – 341, doi:10.1175/2007JCLI1964.1.
- 939 Hanna, E., T. Jonsson and J.E. Box, (2004), An analysis of Icelandic climate since the
 940 nineteenth Century, *Int. J. Clim.*, 24, doi:10.1002/joc.1051.
- 941 Kahn, S.A., A. Aschwanden, A.A. Wahr, K.K. Kjeldsen and K.H. Kjaer, (2015), Greenland
 942 ice sheet mass balance: a review, *Rep. Prog. Phys.* 78, 046801, 26pp.
- 943 Kay, J. E., K. Raeder, A. Gettelman, and J. Anderson (2011), The Boundary Layer
 944 Response to Recent Arctic Sea Ice Loss and Implications for High-Latitude Climate
 945 Feedbacks, *J. Clim.*, 24(2), 428–447, doi:10.1175/2010JCLI3651.1.
- 946 Lefebre, F., Gallée, H., van Ypersele, J.P., and W. Greuell (2003), Modeling of snow and
 947 ice melt at ETH-Camp (West Greenland): A study of surface albedo. *J. Geophys. Res.*,
 948 108(D8), 4231.doi:10.1029/2001JD001160.
- 949 Lefebre, F., Fettweis, X., Galée, H., van Ypersele, J.-P., Marbaix, P., Greuell, W., and P.
 950 Calanca, (2005), Evaluation of a high-resolution regional climate simulation over
 951 Greenland. *Clim. Dyn.*, 25(1), 99–116. doi:10.1007/s00382-005-0005-8.
- 952 Lindsay, R., M. Wensnahan, a. Schweiger, and J. Zhang (2014), Evaluation of Seven
 953 Different Atmospheric Reanalysis Products in the Arctic*, *J. Clim.*, 27(7), 2588–2606,
 954 doi:10.1175/JCLI-D-13-00014.1.
- 955 Liu, J., Z. Chen, J. Francis, M. Song, T. Mote, and Y. Hu (2016), Has Arctic Sea Ice Loss
 956 Contributed to Increased Surface Melting of the Greenland Ice Sheet?, *J. Clim.*, 29(9),
 957 3373–3386, doi:10.1175/JCLI-D-15-0391.1.
- 958 Markus, T., J.C. Stroeve and J. Miller (2009), Recent changes in Arctic sea ice melt onset,
 959 freezeup and melt season length, *J. Geophys. Res.*, 114, C12024,
 960 doi:10.1029/2009JC005436.
- 961 Mattingly, K. S., C. A. Ramseyer, J. J. Rosen, T. L. Mote, and R. Muthyalu (2016),
 962 Increasing water vapor transport to the Greenland Ice Sheet revealed using self-
 963 organizing maps, *Geophys. Res. Lett.*, (August), doi:10.1002/2016GL070424.
- 964 Mioduszewski, J. R., A. K. Rennermalm, A. Hammann, M. Tedesco, E. U. Noble, J. C.
 965 Stroeve, and T. L. Mote (2016), Atmospheric drivers of Greenland surface melt revealed
 966 by self-organizing maps, *J. Geophys. Res. - Atmos.*, 121, 5095–5114,
 967 doi:10.1002/2015JD024550.
- 968 Mortin, J., G. Svensson, R. Graverson, M-L. Kapsch, J.C. Stroeve and L.N. Boisvert
 969 (2016), Melt onset over Arctic sea ice controlled by atmospheric moisture transport,
 970 *Geophys. Res. Lett.*, 43(12), doi:10.1002/2016GL069330.
- 971 Mote, Thomas L. 2014. *MEaSUREs Greenland Surface Melt Daily 25km EASE-Grid 2.0*,
 972 [indicate subset used]. Boulder, Colorado USA: NASA DAAC at the National Snow
 973 and Ice Data Center. doi: <http://dx.doi.org/10.5067/MEASURES/CRYOSPHERE/nsidc-0533.001>
- 975 Mote, Thomas L. 2007. Greenland surface melt trends 1973-2007: Evidence of a large
 976 increase in 2007. *Geophys. Res. Lett.*, 34, L22507. doi:
<http://dx.doi.org/10.1029/2007GL031976>.

- 978 Neff, W., G. Compo, F.M. Ralph and M.D. Shupe (2014), Continental heat anomalies and
 979 the extreme melting of the Greenland ice surface in 2012 and 1889, *J. Geophys. Res.-*
 980 *Atmos.*, doi:10.1002/2014JD021470.
 981 Noël, B., X. Fettweis, W. J. van de Berg, M. R. van den Broeke, and M. Erpicum, 2014:
 982 Sensitivity of Greenland Ice Sheet surface mass balance to perturbations in sea surface
 983 temperature and sea ice cover: a study with the regional climate model MAR. *Cryosph.*,
 984 8, 1871–1883, doi:10.5194/tc-8-1871-2014.
 985 Notz, D. and J. Stroeve (2016), Observed Arctic sea-ice loss directly follows anthropogenic
 986 CO₂ emission, *Science*, doi:10.1126/science.aag2345.
 987 Ornaheim, I.H., T. Eldevik, M. Arthun, R.B. Ingvaldsen and L.H. Smedsrød (2016),
 988 Skillful prediction of Barents Sea ice cover, *Geophys. Res. Lett.*, 42,
 989 doi:10.1002/2015GL064359.
 990 Overland, J. E., and M. Wang (2010), Large-scale atmospheric circulation changes are
 991 associated with the recent loss of Arctic sea ice, *Tellus A*, 62(1), 1–9,
 992 doi:10.1111/j.1600-0870.2009.00421.x.
 993 Parkinson, C. (2014), Spatially mapped reductions in the length of the Arctic sea ice
 994 season, *Geophys. Res. Lett.*, 41(12), doi:10.1002/2014GL060434.
 995 Polyakov, I. V., J. E. Walsh, and R. Kwok (2012), Recent Changes of Arctic Multiyear Sea
 996 Ice Coverage and the Likely Causes, *Bull. Am. Meteorol. Soc.*, 93(2), 145–151,
 997 doi:10.1175/BAMS-D-11-00070.1.
 998 Reichle, R. H., R. D. Koster, G. J. M. De Lannoy, B. a. Forman, Q. Liu, S. P. P.
 999 Mahanama, and A. Touré (2011), Assessment and Enhancement of MERRA Land
 1000 Surface Hydrology Estimates, *J. Clim.*, 24(24), 6322–6338, doi:10.1175/JCLI-D-10-
 1001 05033.1.
 1002 Rennermalm, A.K., L.C. Smith, J.C. Stroeve and V.W.Chu, (2009). Does sea ice
 1003 influenced Greenland ice sheet surface melt?, *Environ. Res. Lett.*, doi:10.1088/1748-
 1004 9326/4/2/024011.
 1005 [Riaz, S.M.F., Iqbal, M.J., and M.J. Baig, \(2017\). Influence of Siberian High on temperature](#)
 1006 [variability over northern areas of South Asia, *Meteorol. Atmos. Phys.*](#)
 1007 [doi:10.1007/s00703-017-0531-z.](#)
 1008 Rienercker, M. M. et al. (2011), MERRA - NASA's Modern-Era Retrospective Analysis for
 1009 Research and Applications, *J. Clim.*, 24, 3624–3648, doi:10.1175/JCLI-D-11-00015.1.
 1010 Rinke, A., W. Maslowski, K. Dethloff, and J. Clement (2006), Influence of sea ice on the
 1011 atmosphere: A study with an Arctic atmospheric regional climate model, *J. Geophys.*
 1012 *Res.*, 111(D16), D16103, doi:10.1029/2005JD006957.
 1013 Screen, J.A. and I. Simmonds (2010), The central role of diminishing sea ice in recent
 1014 Arctic temperature amplification, *Nature*, 464, 1334–1337, doi:10.1038/nature09051.
 1015 Serreze, M.C., J. Stroeve, A.P. Barrett and L.N. Boisvert (2016), Summer atmospheric
 1016 circulation anomalies over the Arctic Ocean and their influences on September sea ice
 1017 extent: A cautionary tale, *J. Geophys. Res. Atmos.*, doi:10.1002/2016JD025161.
 1018 Serreze, M. C., A. P. Barrett, and J. J. Cassano (2011), Circulation and surface controls on
 1019 the lower tropospheric air temperature field of the Arctic, *J. Geophys. Res.*, 116,
 1020 D07104, doi:10.1029/2010JD015127
 1021 Serreze, M.C., A.P. Barrett, J.C. Stroeve, D.N. Kindig and M.M. Holland (2009), The
 1022 emergence of surface-absed Arctic amplification, *The Cryosphere*, 3, 11–19,
 1023 doi:10.5194/tc-3-11.2009.
 1024 Serreze, M.C., M.M. Holland, and J. Stroeve, (2007), Perspectives on the Arctic's
 1025 Shrinking Sea Ice Cover, *Science*, 16, 1533–1536.

- 1026 Stroeve, J.C., A.D. Crawford and S. Stammerjohn (2016), Using timing of ice retreat to
 1027 predict timing of fall freeze-up in the Arctic, *Geophys. Res. Lett.*,
 1028 doi:10.1002/2016GL069314.
- 1029 Stroeve, J.C., T. Markus, L. Boisvert, J. Miller and A. Barrett (2014), Changes in Arctic
 1030 Melt Season and Implications for Sea Ice Loss. *Geophysical Research Letters*,
 1031 doi:10.1002/2013GL058951.
- 1032 Stroeve, J.C., M.C. Serreze, J.E. Kay, M.M. Holland, W.N. Meier and A.P. Barrett, (2012).
 1033 The Arctic's rapidly shrinking sea ice cover: A research synthesis, *Clim. Change*, doi:
 1034 10.1007/s10584-011-0101-1.
- 1035 Stroeve, J. C., M. C. Serreze, A. Barrett, and D. N. Kindig (2011), Attribution of recent
 1036 changes in autumn cyclone associated precipitation in the Arctic, *Tellus A*, 63(4), 653–
 1037 663, doi:10.1111/j.1600-0870.2011.00515.x.
- 1038 Stroeve, J., A. Frei, J. McCreight, and D. Ghatak. 2008. Arctic sea-ice variability revisited.
 1039 *Ann. Glaciol.*, 48(1): 71-81, doi:10.3189/172756408784700699.
- 1040 Tedesco, M., X. Fettweis, P. M. Alexander (2015), MAR v3.2 regional climate model data
 1041 for Greenland (1958-2013). UCAR/NCAR - CISL - ACADIS.
 1042 Dataset.<http://dx.doi.org/10.5065/D6JH3J7Z>.
- 1043 Tedesco, M., X. Fettweis, T. Mote, J. Wahr, P. Alexander, J.E. Box, and B. Wouters,
 1044 (2013), Evidence and analysis of 2012 Greenland records from spaceborne observations,
 1045 a regional climate model and reanalysis data, *The Cryosphere*, 7, 615-630.
- 1046 Tedesco, M. and X. Fettweis (2012), 21st century projections of surface mass balance
 1047 changes for major drainage systems of the Greenland ice sheet, *Env. Res. Lett.*, 7,
 1048 045405.
- 1049 Tedesco, M., X. Fettweis, M. R. van den Broeke, R. S. W. van de Wal, C. J. P. P. Smeets,
 1050 W. J. van de Berg, M. C. Serreze, and J. E. Box (2011), The role of albedo and
 1051 accumulation in the 2010 melting record in Greenland, *Environ. Res. Lett.*, 6(1),
 1052 014005, doi:10.1088/1748-9326/6/1/014005.
- 1053 Tedesco, M. (2007), Snowmelt detection over the Greenland ice sheet from SSM/I
 1054 brightness temperature daily variations, *Geophys. Res. Lett.*, 34, L02504,
 1055 doi:10.1029/2006GL028466.
- 1056 Tedesco, M., M. Serreze, and X. Fettweis (2008), Diagnosing the extreme surface melt
 1057 event over southwestern Greenland in 2007. *Cryos. Disc.* 2(3): 383–397.
- 1058 van den Broeke, M., J. Bamber, J. Ettena, E. Rignot, E. Schrama, W.-J. van de Berg, E. van
 1059 Meijgaard, I. Velicogna and B. Wouters (2009), Partitioning recent Greenland mass
 1060 loss, *Science*, 326, doi:10.1126/science.1178176.
- 1061 van den Broeke, M., and H. Gallée (1996), Observation and simulation of barrier winds at
 1062 the western margin of the Greenland ice sheet, *Q.J.R. Meteorol. Soc.*, 122, 1365-1383.
- 1063 van Tricht, K., and Coauthors, (2016), Clouds enhance Greenland ice sheet meltwater
 1064 runoff, *Nat. Commun.*, 7, 10266, doi:10.1038/ncomms10266.
 1065 <http://www.nature.com/doifinder/10.1038/ncomms10266>.
- 1066 Wang, J., J. Zhang, E. Watanabe, M. Ikeda, K. Mizobata, J.E. Walsh, X. Bai, and B. Wu
 1067 (2009), Is the dipole anomaly a major driver to record lows in Arctic summer sea ice
 1068 extent?, *Geophys. Res. Lett.*, 36, L05706, doi: 10.1029/2008GL036706.
- 1069 [Wallace, J. M., Yuan Zhang, and Kai-Hon Lau \(1993\). Structure and seasonality of
 1070 interannual and interdecadal variability of the geopotential height and temperature fields
 1071 in the Northern Hemisphere troposphere, J. Clim., 6\(11\), 2063–2082, doi:10.1175/1520-
 1072 0442](#)

Formatted: Body A, Indent: Left: 0", Hanging: 0.2", Widow/Orphan control, Adjust space between Latin and Asian text, Adjust space between Asian text and numbers

Formatted: Font:(Default) Times New Roman

1073 Yulaeva, E., N. Schneider, D.W. Pierce, and T.M. Barnett (2001), Modeling of North
1074 Pacific Climate Variability Forced by Oceanic Heat Flux Anomalies, *J. Clim.*, 14, 4027-
1075 4046, doi: 10.1175/1520-0442(2001)014<4027:MONPCV>2.0.CO;2.
1076 Zib, B. J., X. Dong, B. Xi, and A. Kennedy (2012), Evaluation and Intercomparison of
1077 Cloud Fraction and Radiative Fluxes in Recent Reanalyses over the Arctic Using
1078 BSRN Surface Observations, *J. Clim.*, 25(7), 2291–2305, doi:10.1175/JCLI-D-11-
1079 00147.1.
1080

1081
1082
1083
1084
1085
1086
1087

Table 1. Climatological (1981-2010) mean values in length of open water season, together with climatological dates in early melt onset (EMO), continuous melt onset (MO), continuous freeze-up (FO) and melt season duration for 5 sea ice regions (excluding the North Atlantic where little sea ice exists). Corresponding mean dates in melt onset, freeze-up and duration are also shown for the Greenland drainage basins.

Region	Length of Open Water Season (days)	EMO (day of year)	MO (day of year)	FO (day of year)	Melt Duration (days)
<i>Sea Ice Regions</i>					
Baffin Bay	104	146	155	291	136
Davis Strait	220	133	143	321	188
North Atlantic	360	110	134	313	178
Greenland Sea	227	143	148	267	119
Lincoln Sea	0	162	172	232	60
<i>Greenland Ice Sheet Drainage Regions</i>					
Baffin Bay		162	164	232	68
Davis Strait		149	157	247	90
North Atlantic		143	145	234	89
Greenland Sea		163	166	231	65
Lincoln Sea		166	167	230	63

1088
1089

1090 **Table 2.** Trends from 1979 to 2015 in length of open water season, together with trends in
 1091 melt onset, freeze-up and melt season duration for 5 sea ice regions (excluding the North
 1092 Atlantic where little sea ice exists). Corresponding trends in melt onset, freeze-up and
 1093 duration are also shown for the Greenland drainage basins. Only values for the continuous
 1094 melt onset and freeze-up periods are listed. Trends are given as days per decade. Statistical
 1095 significance of trend at 95 and 99% are denoted by ⁺ and ⁺⁺, respectively.
 1096

Region	Open Water Trend (days/dec)	EMO Trend (days/dec)	MO Trend (days/dec)	FO Trend (days/dec)	Melt Duration Trend (days/dec)
<i>Sea Ice Regions</i>					
Baffin Bay	12.6 ⁺	-5.7 ⁺⁺	-8.3 ⁺⁺	7.8 ⁺⁺	16.1 ⁺⁺
Davis Strait	15.9 ⁺	-4.7 ⁺	-6.7 ⁺⁺	5.0 ⁺⁺	11.7 ⁺⁺
North Atlantic	N/A	-6.9 ⁺⁺	-7.3 ⁺⁺	8.9 ⁺⁺	16.3 ⁺⁺
Greenland Sea	15.2 ⁺	-6.7 ⁺⁺	-3.8 ⁺	2.1	5.9 ⁺
Lincoln Sea	-0.1	-4.0 ⁺⁺	-3.9 ⁺⁺	1.6	5.5 ⁺⁺
<i>Greenland Ice Sheet Drainage Regions</i>					
Baffin Bay		-6.1 ⁺⁺	-6.4 ⁺⁺	4.6 ⁺	11.1 ⁺⁺
Davis Strait		-6.3 ⁺⁺	-10.5 ⁺⁺	8.2 ⁺⁺	18.7 ⁺⁺
North Atlantic		-10.7 ⁺⁺	-16.4 ⁺⁺	5.7 ⁺⁺	22.1 ⁺⁺
Greenland Sea		-6.1 ⁺⁺	-6.8 ⁺⁺	7.6 ⁺⁺	14.4 ⁺⁺
Lincoln Sea		-5.1 ⁺⁺	-5.9 ⁺⁺	6.8 ⁺⁺	12.7 ⁺⁺

1097
 1098

1099
1100 **Table 3.** Percentage of grid cells with a significant correlation at $\alpha = 0.05$ relative to the
1101 total grid cells of the unmasked ice sheet. The [Pearson's](#) correlation is between ice sheet
1102 meltwater production and area-averaged sea ice concentration anomalies in the Beaufort
Sea and Baffin Bay (hatched regions in Figures 5a and 6a, respectively).

Month	Beaufort Sea		Baffin Bay	
	Simple Correlation (%)	Partial Correlation (%)	Simple Correlation (%)	Partial Correlation (%)
June	87.0	81.0	17.3	20.2
July	31.2	13.4	11.1	2.1
August	32.6	12.5	12.5	9.4

1103
1104
1105

1106

1107

Table 4. Summary table of results discussed in the main body of the manuscript

Analysis Performed	Davis Strait	Baffin Bay	Lincoln Sea	Greenland Sea	North Atlantic
SVD: GrIS ◇ SIC (Fig. 3)		June			
SIC trends (Fig 4)	Reduced in all seasons	Reduced in all seasons	No change	Positive near the coast in spring and winter	N/A
Open water days (Fig. 4)	Increase	Increase	Increase	Increase	Increase
OWF trends (Fig 5)	Positive throughout shoulder seasons	Sharp peak in June and October	mixed	Positive throughout year, no sharp peaks	N/A
Relative start of melt on SIC and GrIS (table 2)	SIC MO earlier, SIC FO later	SIC MO earlier, SIC FO later	SIC and GrIS similar	SIC MO earlier, SIC FO later	N/A
Trends in timing of EMO, MO, FO (table 2, Figure 6)	MO earlier FO later	MO earlier FO later	MO earlier FO later	MO earlier FO later	N/A
Synchronicity between GrIS and SIC EMO, MO, FO time series		R>0.6 for MO, FO R> 0.5 for detrended data	R>0.6 for MO, FO R> 0.5 for detrended data	R > 0.5 for EMO	
Latent heat fluxes (Fig 7)	positive all year	positive all year	positive in summer	positive all year	N/A
Sensible heat fluxes (Fig. 7)	Positive spring/fall	Positive JASO	Negative all year	Positive spring/fall	N/A
Early/late MO years composites (Fig 7)	Positive in winter, negative rest of year	Majority of positive anomalies	mixed	mixed	
Net longwave fluxes (Fig. 8)	Positive anomalies in spring	Positive anomalies in spring	Positive anomalies in spring	Positive anomalies in spring	N/A

1108

1109

1110

1111

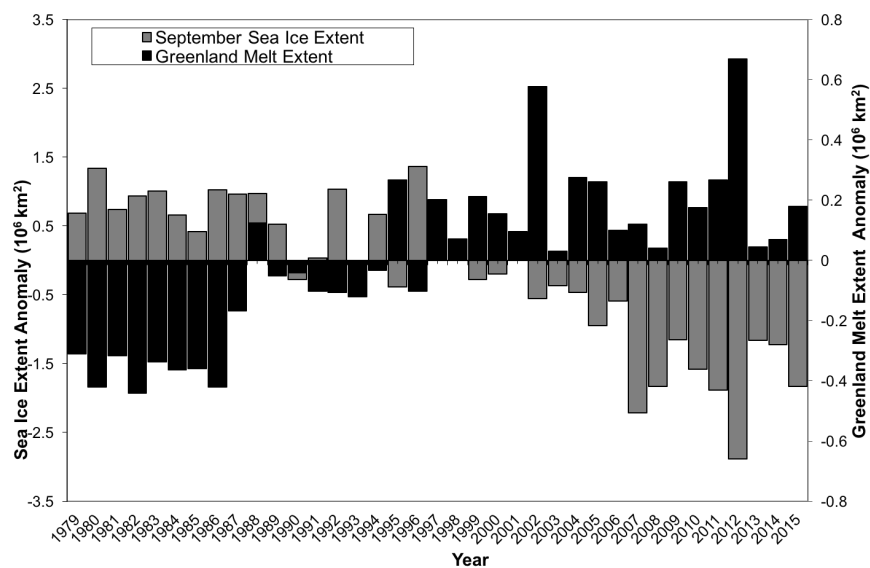
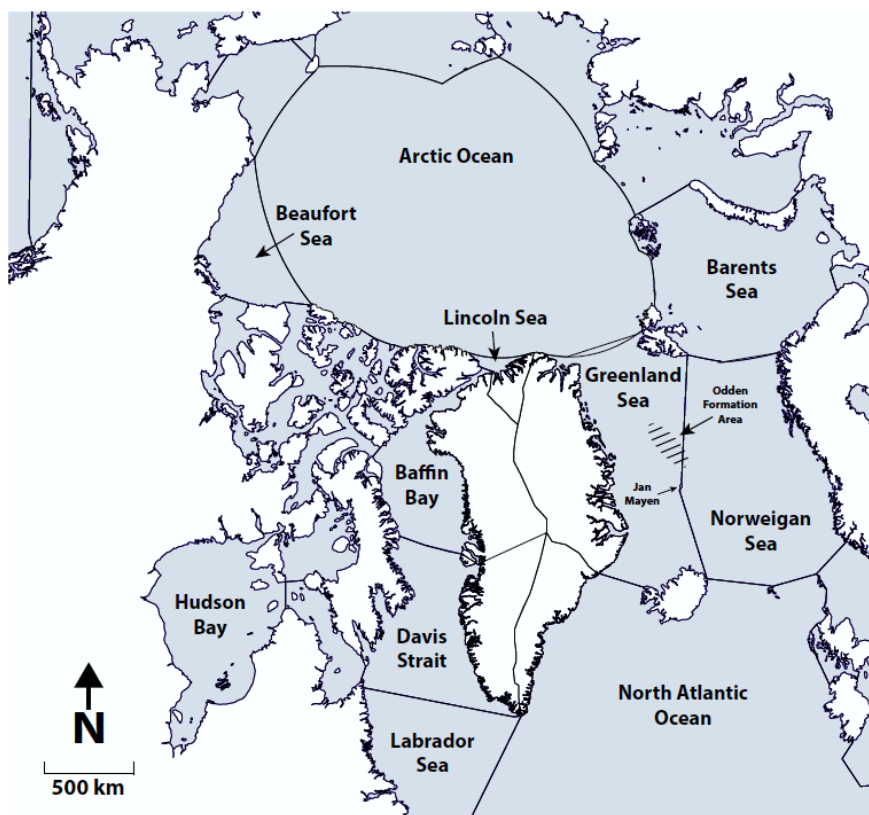


Figure 1. Time-series of September sea ice extent and Greenland surface melt extent anomalies from 1979 to 2015.



1118

1119

1120

1121

1122

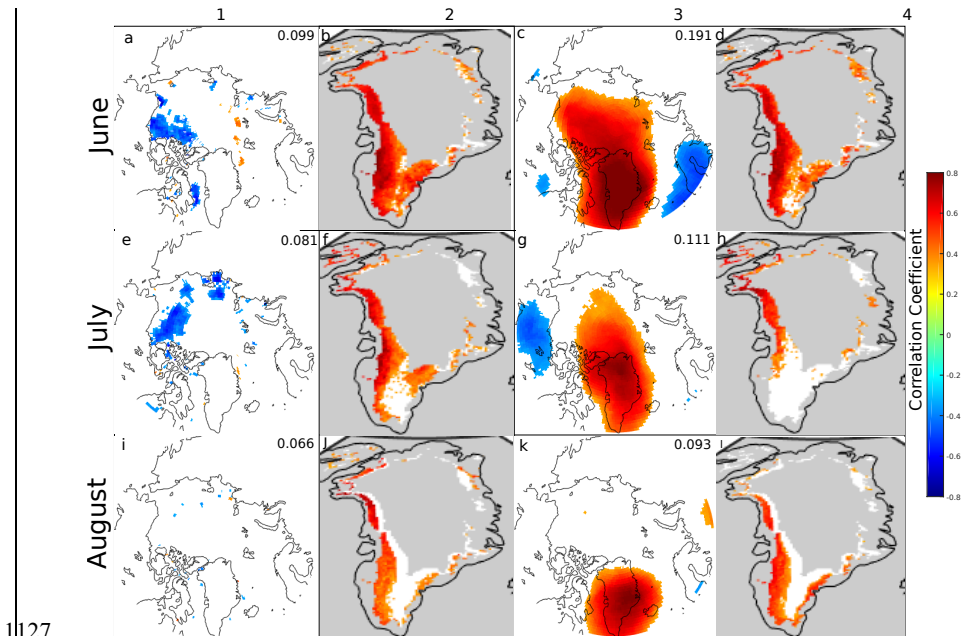
1123

1124

1125

1126

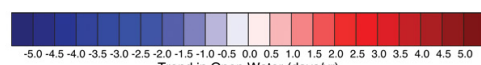
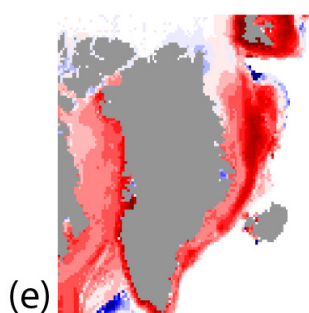
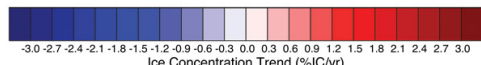
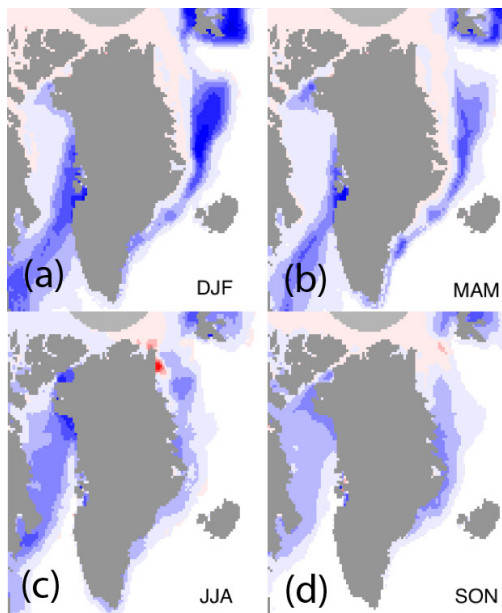
Figure 2. Map of study area, including the six sea ice and Greenland drainage sectors used in this study. The ice sheet regions are named after their adjacent sea (i.e. Davis Strait, Baffin Bay, Lincoln Sea, Greenland Sea, and the North Atlantic). The approximate area where the Odden sea ice featured used to formed is indicated with hatched lines. The ocean boundaries are defined by the International Hydrographic Organization (VLIZ (2005). IHO Sea Areas. Available online at <http://www.marineregions.org/.>



Deleted: <sp>

Formatted: Font:TimesNewRoman

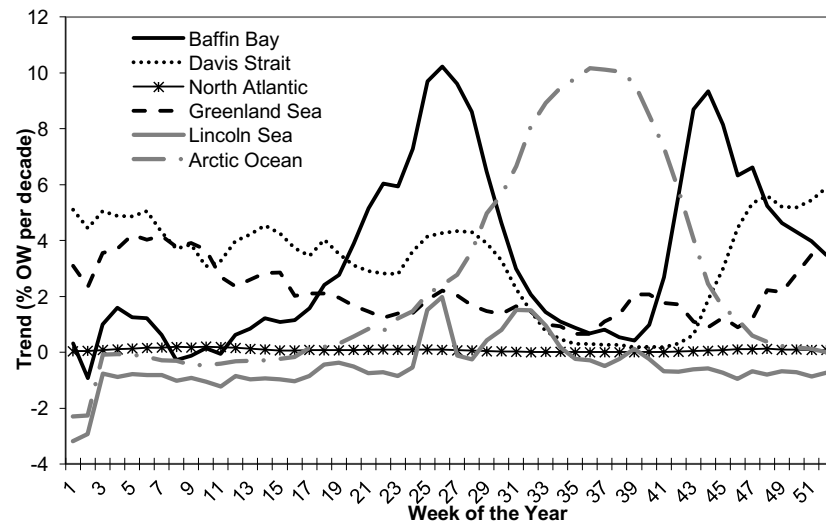
1|127
1|128 **Figure 3.** Heterogeneous correlation between variables in the leading SVD mode in
1|129 JJA. Column 1 is the correlation between sea ice concentration and EC_{GrIS} . Column 2 is
1|130 the correlation between meltwater production and EC_{SIC} . Column 3 is the correlation
1|131 between 500 hPa geopotential heights and EC_{GrIS} . Column 4 is the correlation between
1|132 meltwater production and the EC_{500} . Correlation coefficients are not considered over
1|133 the masked gray regions, and only correlations significant at $\alpha = 0.05$ are shown. [The
1|134 normalized squared covariance \(NSC\) is given in the upper right of columns 1 and 3.](#)
1|135 All data are anomalies relative to 1979-2015 means with the least-squares trend line
1|136 removed.
1|137
1|138



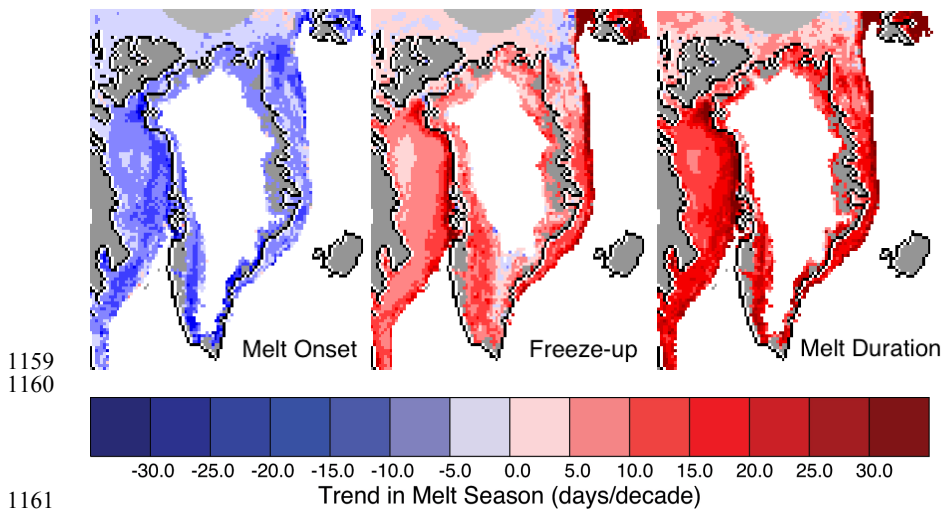
1140
 1141
 1142
 1143
 1144
 1145
 1146

Figure 4. Seasonal trends in sea ice concentration from 1979 to 2015 (a-d) and number of ice free days (e). Trends are computed using linear least squares and evaluated using student T-test at 95% confidence interval.

1147
1148

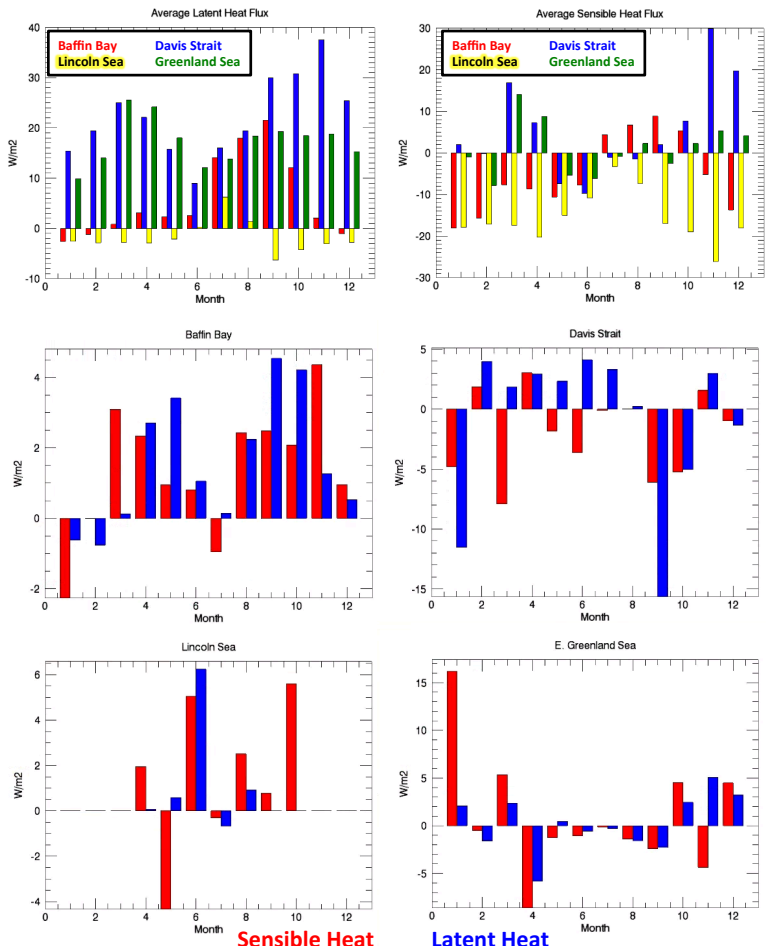


1149
1150
1151
1152
1153 Trends in regional open water fraction (OWF) surrounding the Greenland
1154 Ice Sheet, computed from 1979 to 2014. [Trends are computed using linear least](#)
1155 [squares.](#)



1161
1162
1163 **Figure 6.** Trends in melt onset (left), freeze-up (middle) and total melt season length
1164 (right) for sea ice and Greenland from 1979 to 2015. Trends are computed using
1165 linear least squares and evaluated at the 95% confidence level using student T-test.
1166

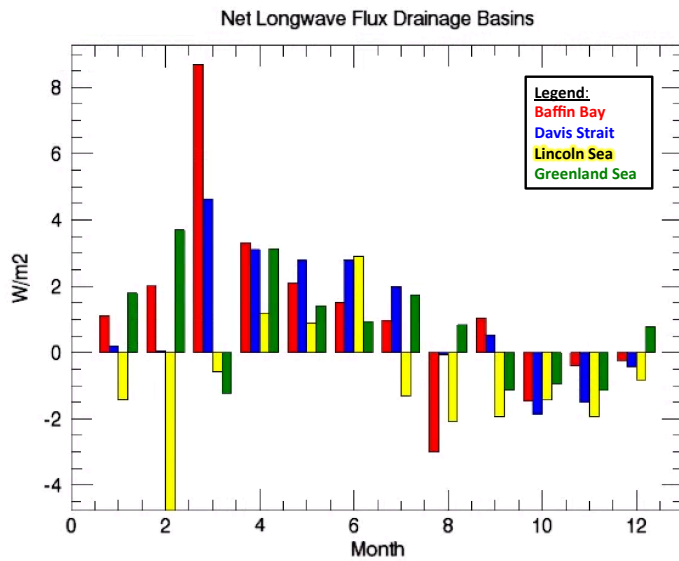
Deleted: top
Deleted: bottom



1169
1170
1171
1172
1173
1174

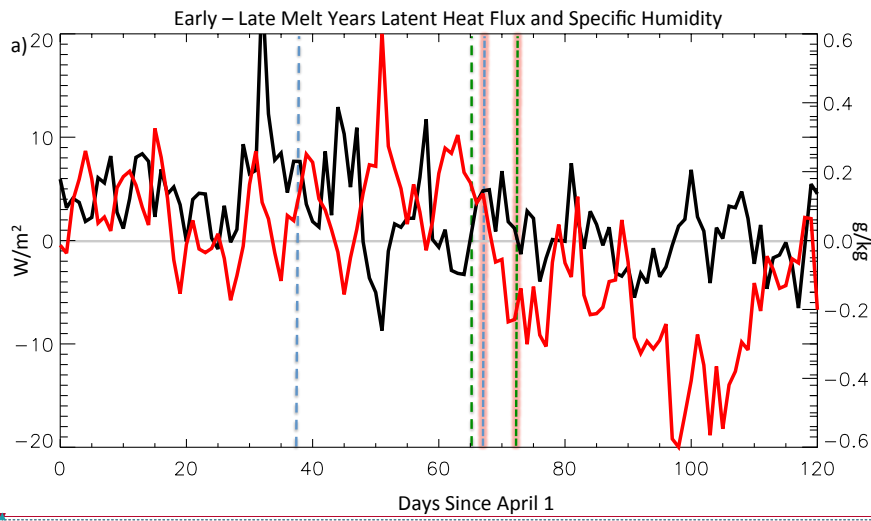
Figure 7. Top row graphs show the 2002 to 2015 average latent and sensible heat fluxes for each ocean region (denoted by color). The sign convention is such that positive fluxes are directed from the ocean to the atmosphere. Bottom two row

1175 graphs show the early minus late melt onset years for each region of the positive (into
1176 the atmosphere) sensible (red) and latent (blue) heat fluxes.
1177
1178
1179



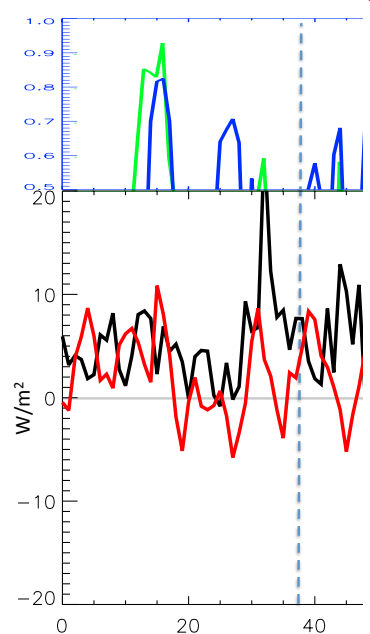
1180
1181
1182 **Figure 8.** Net longwave flux (downwelling longwave flux – upwelling longwave flux)
1183 for early MO minus late MO years for the drainage basins of the Greenland Ice Sheet,
1184 where red bars are for Baffin Bay, blue bars are for Davis Strait, yellow bars are for
1185 Lincoln Sea and green bars and for Greenland sea.
1186

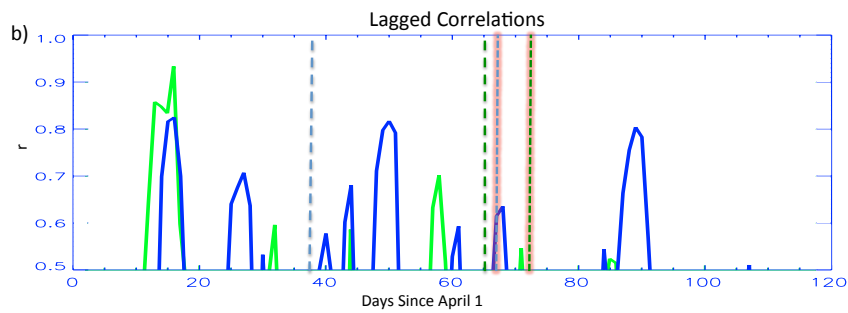
1187
1188
1189



1190
1191
1192
1193
1194
1195
1196
1197

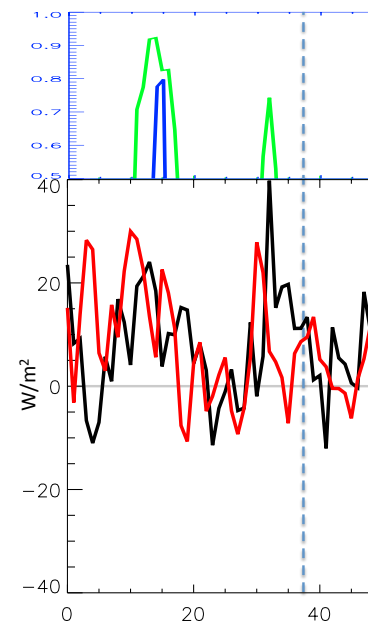
Figure 9a. Baffin Bay SIC region latent heat flux from early minus late MO years (black line) and Baffin Bay GrIS region specific humidity from early minus late MO years (red line). Dotted vertical lines represent the average early melt onset date for Baffin Bay (dotted blue), and average late melt onset date for Baffin Bay (dotted blue, red highlight), average early melt onset date for GrIS (dotted green), and average late melt onset date for GrIS (dotted green, orange highlight).





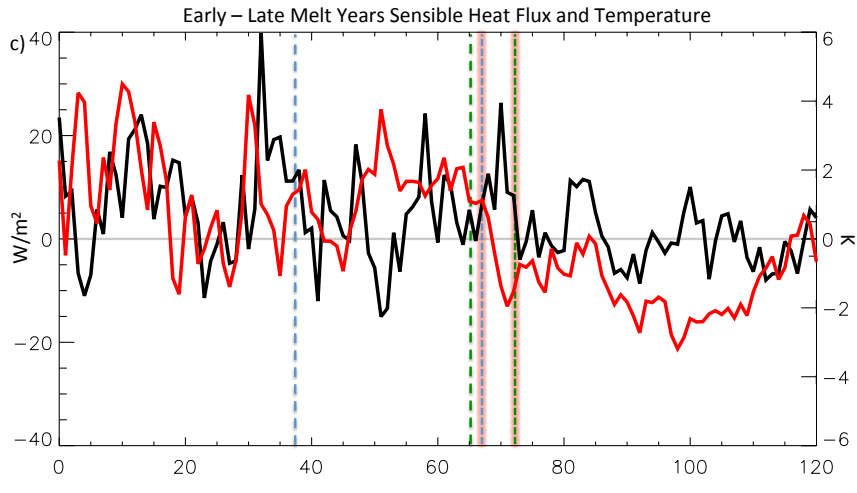
Formatted: Font:TimesNewRoman

1|199
1|200 **Figure 9b.** Week lag-1 week lagged running correlations (between 0.5 and 1.0) for
1|201 early melt years latent heat flux from Baffin Bay and specific humidity from GrIS
1|202 (blue) and late melt onset latent heat flux from Baffin Bay and specific humidity from
1|203 GrIS years (green).
1|204
1|205



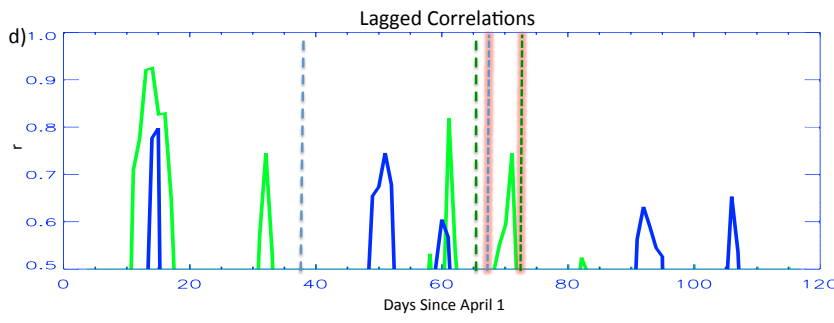
Formatted: Font:Bold

Deleted: The top portion of this figure shows the w



Deleted: 9b

1208
1209 **Figure 9c.** Baffin Bay SIC region sensible heat flux from early minus late MO years
1210 (black line) and Baffin Bay GrIS region air temperature from early minus late MO
1211 years (red line). Dotted vertical lines represent the average early melt onset date for
1212 Baffin Bay (dotted blue), and average late melt onset date for Baffin Bay (dotted
1213 green), average early melt onset date for GrIS (dotted blue, red highlight), and
1214 average late melt onset date for GrIS (dotted green, orange highlight).



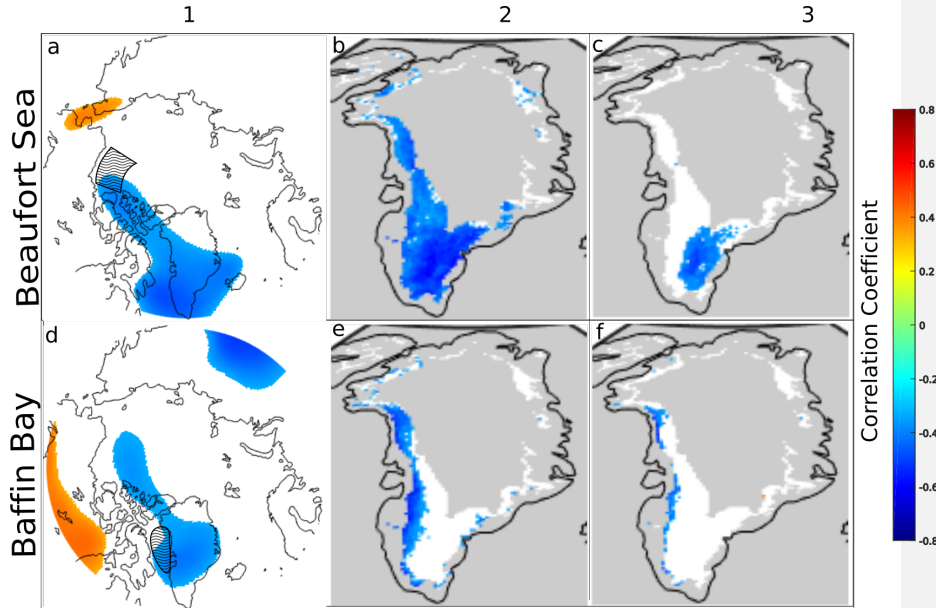
Formatted: Font:TimesNewRoman

1216
1217 **Figure 9d.** Week lag-1 week lagged running correlations (between 0.5 and 1.0) for
1218 early years sensible heat flux from Baffin Bay and air temperature from GrIS (blue)
1219 and late melt onset sensible heat flux from Baffin Bay and air temperature from GrIS
1220 years (green).
1221

Formatted: Font:Bold

Deleted: The top portion of this figure shows the w

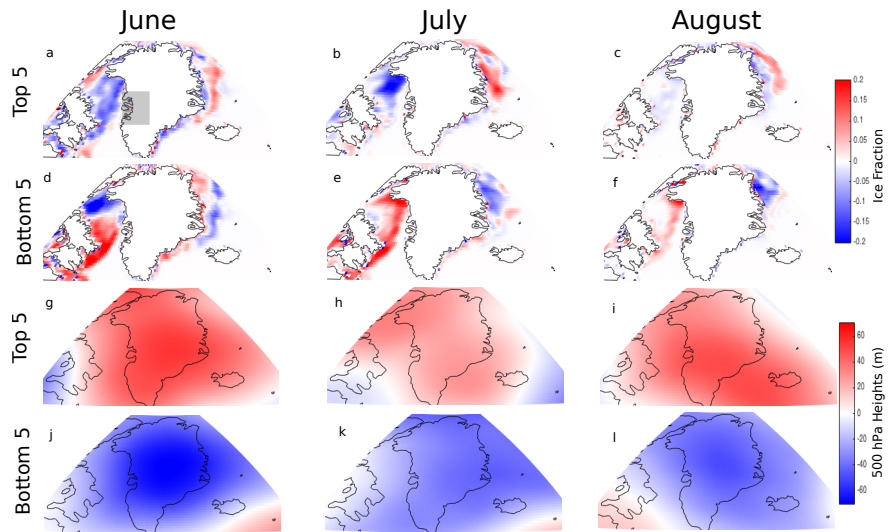
1223
1224
1225
1226
1227



1228
1229
1230
1231
1232
1233
1234
1235
Figure 10. June correlation between spatially averaged SIC in the hatched region and:
Column 1) 500 hPa geopotential height field, Column 2) Greenland meltwater
production, and Column 3) same as Column 2 but with the effect of the Greenland
Blocking Index removed (partial correlation). Correlation coefficients are not
considered over the masked gray regions. All data are anomalies relative to 1979-
2015 means with the least-squares trend line removed.

1236

1237



Deleted:

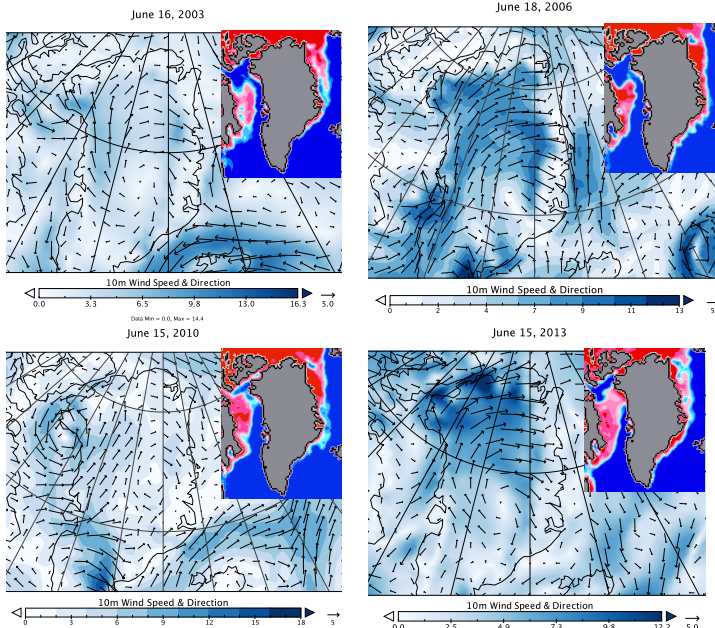
Formatted: Font:TimesNewRoman

1238
1239 **Figure 11.** De-trended anomalies of SIC (a-f) and 500 hPa geopotential heights (g-l)
1240 averaged over the 5 highest and lowest melt years in June, July, and August as
1241 indicated by de-trended meltwater production anomalies in the indicated gray region
1242 of the ice sheet. Units are ice fraction (a-f) and m (g-l).

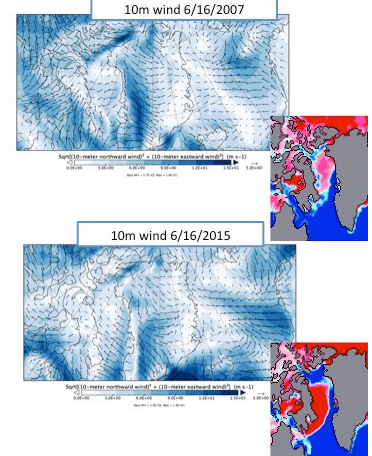
1243

1244

1246
1247

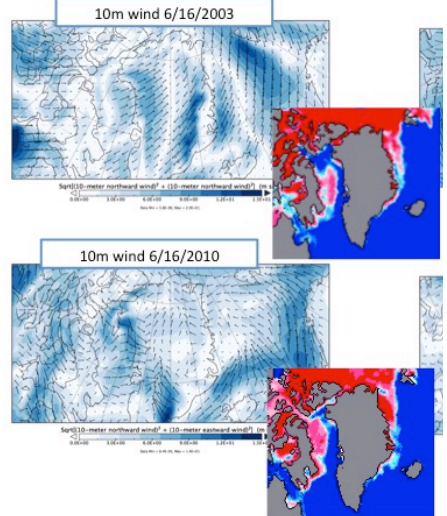


Formatted: Font:(Default) TimesNewRoman, Font color: Black



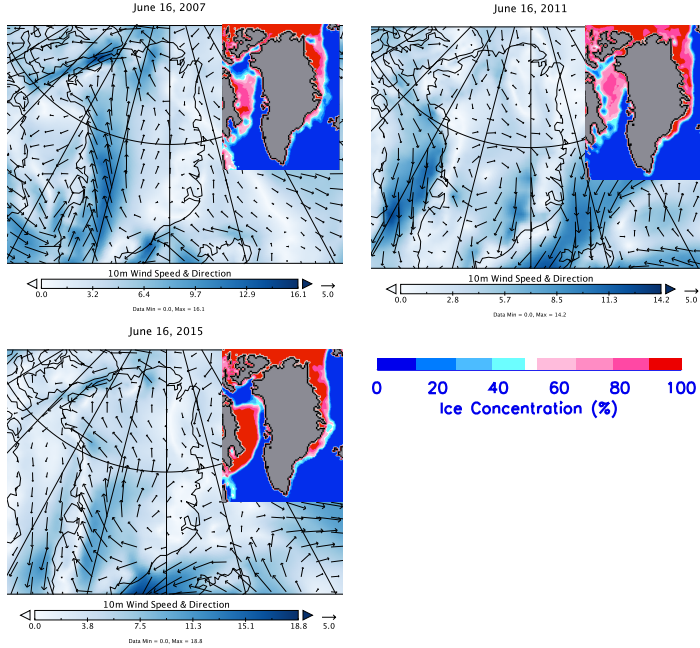
Late Melt Years

Deleted:



Formatted: Font:TimesNewRoman

Formatted: Font:TimesNewRoman, Bold



1250
1251 **Figure 12.** Wind vectors and speeds at 10 meters from MERRA-2 during 4 early sea
1252 melt years over Baffin Bay (top panel) and 3 late sea melt years (bottom) panel.
1253 Smaller figures superimposed on the wind maps show the sea ice concentration (%)
1254 for that day.
1255

Deleted: Daily w
Deleted: AIRS
Deleted: 3
Deleted: 4